receptors results in phosphorylation of CREB (cAMP-response-element-binding protein) [45]. We showed that approx. 70% of both small-sized DRG neurons and NHEKs possess functional $P2Y_2$ receptors in the co-culture (Figure 5). In the peripheral skin-to-sensory neuron system, $P2Y_2$ receptors might be the main sensor for both NHEKs and DRG neurons. However, we cannot exclude the possibility that Ca^{2+} entry via P2X receptors is also involved in Ca^{2+} signalling in DRG neurons. In fact, when skin cells are killed, a large amount of intracellular ATP in the skin leaks and excites nociceptors by activating P2X receptors [46]. In a skin–nerve preparation, carrageenan inflammation of skin resulted in an increase in the activities of c-fibres, which was mediated by P2X receptors [47]. There might be multiple mechanisms by which the skin communicates with sensory neurons through ATP.

Apart from those of cell injury, the mechanisms underlying ATP release from NHEKs remain unknown. In neuronal cells, depolarizing stimulation resulted in exocytotic release of ATP in hippocampal slices [48] and cultured hippocampal neurons [49]. However, in non-excitable cells including NHEKs, the mechanism of ATP release is still a matter of debate. In astrocytes, there have been several reports that ATP can be released via chloride channels [50], gap junction hemi-channels [51], ATP-binding cassette [52] and exocytosis [53,54]. NHEKs also express several types of chloride channels [34,55,56], connexins [57–59] and SNARE (soluble *N*-ethylmaleimide-sensitive fusion protein attachment protein receptor) proteins [60,61]. Although these similarities raise the possibility that NHEKs and astrocytes might share the same mechanism for the release of ATP, further investigation is needed.

In summary, we demonstrated that extracellular ATP derived from NHEKs functions in both an autocrine and paracrine manner in the peripheral skin-to-sensory neurons system. Metabotropic $P2Y_2$ receptors may be important sensors for extracellular ATP in both NHEKs and small-sized DRG neurons.

We thank T. Obama (Division of Biosignaling, National Institute of Health Sciences) for helping in the culturing of cells and Y. Ohno (Division of Pharmacology, National Institute of Health Sciences) for continuous encouragement. This work was partially supported by the Organization for Pharmaceutical Safety and Research (Medical Frontier Project; MF-16), the Health Science Foundation (Japan) and Shiseido Research Center (Yokohama, Japan).

REFERENCES

1 Denda, M., Fuziwara, S., Inoue, K., Denda, S., Akamatsu, H., Tomitaka, A. and Matsunaga, K. (2001) Immunoreactivity of VR1 on epidermal keratinocyte of human skin. Biochem. Biophys. Res. Commun. **285**, 1250–1252
2 Inoue, K., Koizumi, S., Fuziwara, S., Denda, S. and Denda, M. (2002) Functional vanilloid receptors in cultured normal human epidermal keratinocytes. Biochem. Biophys. Res. Commun. **291**, 124–129
3 Grando, S. A. (1997) Biological functions of keratinocyte cholinergic receptors. J. Investig. Dermatol. Symp. Proc. **2**, 41–48
4 Arredondo, J., Nguyen, V. T., Chernyavsky, A. I., Bercovich, D., Orr-Urtreger, A., Kummer, W., Lips, K., Vetter, D. E. and Grando, S. A. (2002) Central role of α7 nicotinic receptor in differentiation of the stratified squamous epithelium. J. Cell Biol. **159**, 325–336
5 Genever, P. G., Maxfield, S. J., Kennovin, G. D., Maltman, J., Bowgen, C. J., Raxworthy, M. J. and Skerry, T. M. (1999) Evidence for a novel glutamate-mediated signaling pathway in keratinocytes. J. Invest. Dermatol. **112**, 337–342
6 Dixon, C. J., Bowler, W. B., Littlewood-Evans, A., Dillon, J. P., Bilbe, G., Sharpe, G. R. and Gallagher, J. A. (1999) Regulation of epidermal homeostasis through P2Y2 receptors. Br. J. Pharmacol. **127**, 1680–1686
7 Stoebner, P. E., Carayon, P., Penarier, G., Frechin, N., Barneon, G., Casellas, P., Cano, J. P., Meynadier, J. and Meunier, L. (1999) The expression of peripheral benzodiazepine receptors in human skin: the relationship with epidermal cell differentiation. Br. J. Dermatol. **140**, 1010–1016
8 Zia, S., Ndoye, A., Lee, T. X., Webber, R. J. and Grando, S. A. (2000) Receptor-mediated inhibition of keratinocyte migration by nicotine involves modulations of calcium influx and intracellular concentration. J. Pharmacol. Exp. Ther. **293**, 973–981
9 Watt, F. M., Hudson, D. L., Lamb, A. G., Bolsover, S. R., Silver, R. A., Aitchison, M. J. and Whitaker, M. (1991) Mitogens induce calcium transients in both dividing and terminally differentiating keratinocytes. J. Cell Sci. **99**, 397–405
10 Cornell-Bell, A. H., Finkbeiner, S. M., Cooper, M. S. and Smith, S. J. (1990) Glutamate induces calcium waves in cultured astrocytes: long-range glial signaling. Science **247**, 470–473
11 Charles, A. C., Merrill, J. E., Dirksen, E. R. and Sanderson, M. J. (1991) Intercellular signaling in glial cells: calcium waves and oscillations in response to mechanical stimulation and glutamate. Neuron **6**, 983–992
12 Thomas, A. P., Renard, D. C. and Rooney, T. A. (1991) Spatial and temporal organization of calcium signalling in hepatocytes. Cell Calcium **12**, 111–126
13 Hansen, M., Boitano, S., Dirksen, E. R. and Sanderson, M. J. (1993) Intercellular calcium signaling induced by extracellular adenosine 5′-triphosphate and mechanical stimulation in airway epithelial cells. J. Cell Sci. **106**, 995–1004
14 Demer, L. L., Wortham, C. M., Dirksen, E. R. and Sanderson, M. J. (1993) Mechanical stimulation induces intercellular calcium signaling in bovine aortic endothelial cells. Am. J. Physiol. **264**, H2094–H2102
15 Guthrie, P. B., Knappenberger, J., Segal, M., Bennett, M. V., Charles, A. C. and Kater, S. B. (1999) ATP released from astrocytes mediates glial calcium waves. J. Neurosci. **19**, 520–528
16 Scemes, E., Dermietzel, R. and Spray, D. C. (1998) Calcium waves between astrocytes from Cx43 knockout mice. Glia **24**, 65–73
17 Cauna, N. (1973) The free penicillate nerve endings of the human hairy skin. J. Anat. **115**, 277–288
18 Hilliges, M., Wang, L. and Johansson, O. (1995) Ultrastructural evidence for nerve fibers within all vital layers of the human epidermis. J. Invest. Dermatol. **104**, 134–137
19 Peier, A. M., Reeve, A. J., Andersson, D. A., Moqrich, A., Earley, T. J., Hergarden, A. C., Story, G. M., Colley, S., Hogenesch, J. B., McIntyre, P. et al. (2002) A heat-sensitive TRP channel expressed in keratinocytes. Science **296**, 2046–2049
20 Hensel, H. and Iggo, A. (1971) Analysis of cutaneous warm and cold fibres in primates. Pflugers Arch. **329**, 1–8
21 Hensel, H. and Kenshalo, D. R. (1969) Warm receptors in the nasal region of cats. J. Physiol. (Cambridge, U.K.) **204**, 99–112
22 Grynkiewicz, G., Poenie, M. and Tsien, R. Y. (1985) A new generation of Ca^{2+} indicators with greatly improved fluorescence properties. J. Biol. Chem. **260**, 3440–3450
23 Koizumi, S., Rosa, P., Willars, G. B., Challiss, R. A., Taverna, E., Francolini, M., Bootman, M. D., Lipp, P., Inoue, K., Roder, J. et al. (2002) Mechanisms underlying the neuronal calcium sensor-1-evoked enhancement of exocytosis in PC12 cells. J. Biol. Chem. **277**, 30315–30324
24 Koizumi, S., Bootman, M. D., Bobanovic, L. K., Schell, M. J., Berridge, M. J. and Lipp, P. (1999) Characterization of elementary Ca^{2+} release signals in NGF-differentiated PC12 cells and hippocampal neurons. Neuron **22**, 125–137
25 Communi, D., Pirotton, S., Parmentier, M. and Boeynaems, J. M. (1995) Cloning and functional expression of a human uridine nucleotide receptor. J. Biol. Chem. **270**, 30849–30852
26 Chang, K., Hanaoka, K., Kumada, M. and Takuwa, Y. (1995) Molecular cloning and functional analysis of a novel P2 nucleotide receptor. J. Biol. Chem. **270**, 26152–26158
27 Communi, D., Parmentier, M. and Boeynaems, J. M. (1996) Cloning, functional expression and tissue distribution of the human P2Y6 receptor. Biochem. Biophys. Res. Commun. **222**, 303–308
28 Communi, D., Motte, S., Boeynaems, J. M. and Pirotton, S. (1996) Pharmacological characterization of the human P2Y4 receptor. Eur. J. Pharmacol. **317**, 383–389
29 Greig, A. V., Linge, C., Terenghi, G., McGrouther, D. A. and Burnstock, G. (2003) Purinergic receptors are part of functional signaling system for proliferation and differentiation of human epidermis keratinocytes. J. Invest. Dermatol. **120**, 1007–1015
30 Fam, S. R., Gallagher, C. J. and Salter, M. W. (2000) P2Y1 purinoceptor-mediated Ca^{2+} signaling and Ca^{2+} wave propagation in dorsal spinal cord astrocytes. J. Neurosci. **20**, 2800–2808
31 Newman, E. A. and Zahs, K. R. (1998) Modulation of neuronal activity by glial cells in the retina. J. Neurosci. **18**, 4022–4028
32 Finkbeiner, S. (1992) Calcium waves in astrocytes – filling in the gaps. Neuron **8**, 1101–1108
33 Burgstahler, R., Koegel, H., Rucker, F., Tracey, D., Grafe, P. and Alzheimer, C. (2003) Confocal ratiometric voltage imaging of cultured human keratinocytes reveals layer-specific responses to ATP. Am. J. Physiol. **284**, C944–C952
34 Koegel, H. and Alzheimer, C. (2001) Expression and biological significance of Ca^{2+}-activated ion channels in human keratinocytes. FASEB J. **15**, 145–154

35 Denda, M., Inoue, K., Fuziwara, S. and Denda, S. (2002) P2X purinergic receptor antagonist accelerates skin barrier repair and prevents epidermal hyperplasia induced by skin barrier disruption. J. Invest. Dermatol. **119**, 1034–1040
36 Koizumi, S., Fujishita, K., Tsuda, M., Shigemoto-Mogami, Y. and Inoue, K. (2003) Dynamic inhibition of excitatory synaptic transmission by astrocyte-derived ATP in hippocampal cultures. Proc. Natl. Acad. Sci. U.S.A. **100**, 11023–11028
37 Newman, E. A. (2003) Glial cell inhibition of neurons by release of ATP. J. Neurosci. **23**, 1659–1666
38 Tsuda, M., Shigemoto-Mogami, Y., Koizumi, S., Mizokoshi, A., Kohsaka, S., Salter, M. W. and Inoue, K. (2003) P2X4 receptors induced in spinal microglia gate tactile allodynia after nerve injury. Nature (London) **424**, 778–783
39 Cervero, F. (1994) Sensory innervation of the viscera: peripheral basis of visceral pain. Physiol. Rev. **74**, 95–138
40 Nakamura, F. and Strittmatter, S. M. (1996) P2Y1 purinergic receptors in sensory neurons: contribution to touch-induced impulse generation. Proc. Natl. Acad. Sci. U.S.A. **93**, 10465–10470
41 Burnstock, G. (2000) P2X receptors in sensory neurones. Br. J. Anaesth. **84**, 476–488
42 Tsuda, M., Koizumi, S., Kita, A., Shigemoto, Y., Ueno, S. and Inoue, K. (2000) Mechanical allodynia caused by intraplantar injection of P2X receptor agonist in rats: involvement of heteromeric P2X2/3 receptor signaling in capsaicin-insensitive primary afferent neurons. J. Neurosci. **20**, RC90
43 Tominaga, M., Wada, M. and Masu, M. (2001) Potentiation of capsaicin receptor activity by metabotropic ATP receptors as a possible mechanism for ATP-evoked pain and hyperalgesia. Proc. Natl. Acad. Sci. U.S.A. **98**, 6951–6956
44 Sanada, M., Yasuda, H., Omatsu-Kanbe, M., Sango, K., Isono, T., Matsuura, H. and Kikkawa, R. (2002) Increase in intracellular Ca^{2+} and calcitonin gene-related peptide release through metabotropic P2Y receptors in rat dorsal root ganglion neurons. Neuroscience **111**, 413–422
45 Molliver, D. C., Cook, S. P., Carlsten, J. A., Wright, D. E. and McCleskey, E. W. (2002) ATP and UTP excite sensory neurons and induce CREB phosphorylation through the metabotropic receptor, P2Y2. Eur. J. Neurosci. **16**, 1850–1860
46 Cook, S. P. and McCleskey, E. W. (2002) Cell damage excites nociceptors through release of cytosolic ATP. Pain **95**, 41–47
47 Hamilton, S. G., McMahon, S. B. and Lewin, G. R. (2001) Selective activation of nociceptors by P2X receptor agonists in normal and inflamed rat skin. J. Physiol. (Cambridge, U.K.) **534**, 437–445
48 Wieraszko, A., Goldsmith, G. and Seyfried, T. N. (1989) Stimulation-dependent release of adenosine triphosphate from hippocampal slices. Brain Res. **485**, 244–250
49 Koizumi, S., Fujishita, K., Tsuda, M. and Inoue, K. (2003) Neuron-to-astrocyte communication by endogenous ATP in mixed culture of rat hippocampal neurons and astrocyte. Drug Dev. Res. **59**, 88–94
50 Darby, M., Kuzmiski, J. B., Panenka, W., Feighan, D. and MacVicar, B. A. (2003) ATP released from astrocytes during swelling activates chloride channels. J. Neurophysiol. **89**, 1870–1877
51 Stout, C. E., Costantin, J. L., Naus, C. C. and Charles, A. C. (2002) Intercellular calcium signaling in astrocytes via ATP release through connexin hemichannels. J. Biol. Chem. **277**, 10482–10488
52 Ballerini, P., Di Iorio, P., Ciccarelli, R., Nargi, E., D'Alimonte, I., Traversa, U., Rathbone, M. P. and Caciagli, F. (2002) Glial cells express multiple ATP binding cassette proteins which are involved in ATP release. Neuroreport **13**, 1789–1792
53 Maienschein, V., Marxen, M., Volknandt, W. and Zimmermann, H. (1999) A plethora of presynaptic proteins associated with ATP-storing organelles in cultured astrocytes. Glia **26**, 233–244
54 Coco, S., Calegari, F., Pravettoni, E., Pozzi, D., Taverna, E., Rosa, P., Matteoli, M. and Verderio, C. (2003) Storage and release of ATP from astrocytes in culture. J. Biol. Chem. **278**, 1354–1362
55 Galietta, L. J., Barone, V., de Luca, M. and Romeo, G. (1991) Characterization of chloride and cation channels in cultured human keratinocytes. Pflugers Arch. **418**, 18–25
56 Mastrocola, T., de Luca, M. and Rugolo, M. (1991) Characterization of chloride transport pathways in cultured human keratinocytes. Biochim. Biophys. Acta **1097**, 275–282
57 Risek, B. and Gilula, N. B. (1991) Spatiotemporal expression of three gap junction gene products involved in fetomaternal communication during rat pregnancy. Development **113**, 165–181
58 Di, W. L., Rugg, E. L., Leigh, I. M. and Kelsell, D. P. (2001) Multiple epidermal connexins are expressed in different keratinocyte subpopulations including connexin 31. J. Invest. Dermatol. **117**, 958–964
59 Plum, A., Hallas, G. and Willecke, K. (2002) Expression of the mouse gap junction gene Gjb3 is regulated by distinct mechanisms in embryonic stem cells and keratinocytes. Genomics **79**, 24–30
60 Scott, G. and Zhao, Q. (2001) Rab3a and SNARE proteins: potential regulators of melanosome movement. J. Invest. Dermatol. **116**, 296–304
61 Scott, G., Leopardi, S., Printup, S. and Madden, B. C. (2002) Filopodia are conduits for melanosome transfer to keratinocytes. J. Cell Sci. **115**, 1441–1451

Received 21 July 2003/23 December 2003; accepted 16 February 2004
Published as BJ Immediate Publication 16 February 2004, DOI 10.1042/BJ20031089

Cellular/Molecular

Production and Release of Neuroprotective Tumor Necrosis Factor by $P2X_7$ Receptor-Activated Microglia

Tomohisa Suzuki,[1] Izumi Hide,[1] Katsutoshi Ido,[1] Shinichi Kohsaka,[2] Kazuhide Inoue,[3,4] and Yoshihiro Nakata[1]

[1]Department of Pharmacology, Graduate School of Biomedical Sciences, Hiroshima University, Hiroshima 734-8551, Japan, [2]Department of Neurochemistry, National Institute of Neuroscience, Tokyo 187-8502, Japan, [3]Division of Biosignaling, National Institute of Health Science, Tokyo 158-8501, Japan, and [4]Graduate School of Pharmaceutical Sciences, Kyushu University, Fukuoka 812-8582, Japan

After a brain insult, ATP is released from injured cells and activates microglia. The microglia that are activated in this way then release a range of bioactive substances, one of which is tumor necrosis factor (TNF). The release of TNF appears to be dependent on the $P2X_7$ receptor. The inhibitors 1,4-diamino-2,3-dicyano-1,4-bis[2-amino-phenylthio]butadiene (U0126), anthra[1,9-cd]pyrazol-6(2H)-one (SP600125), and 4-(4-fluorophenyl)-2-(4-methylsulfinylphenyl)-5-(4-pyridyl)IH-imidazole (SB203580), which target MEK (mitogen-activated protein kinase kinase), JNK (c-Jun N-terminal kinase), and p38, respectively, all potently suppress the production of TNF in ATP-stimulated microglia, whereas the production of TNF mRNA is strongly inhibited by U0126 and SP600125. SB203580 did not affect the increased levels of TNF mRNA but did prevent TNF mRNA from accumulating in the cytoplasm. The ATP-provoked activation of JNK and p38 [but not extracellular signal-regulated kinase (ERK)] could be inhibited by brilliant blue G, a $P2X_7$ receptor blocker, and by genistein and 4-amino-5-(4-chlorophenyl)-7-(*t*-butyl)pyrazolo[3,4-D]pyrimidine, which are general and *src*-family-specific tyrosine kinase inhibitors, respectively. Most important, we found that treatment of the microglia in neuron–microglia cocultures with the $P2X_7$ agonist 2′–3′-*O*-(benzoyl-benzoyl) ATP led to significant reductions in glutamate-induced neuronal cell death, and that either TNF-α converting enzyme inhibitor or anti-TNF readily suppressed the protective effect implied by this result. Together, these findings indicate that both ERK and JNK are involved in the regulation of TNF mRNA expression, that p38 is involved in the nucleocytoplasmic transport of TNF mRNA, and that a PTK (protein tyrosine kinase), possibly a member of the *src* family, acts downstream of the $P2X_7$ receptor to activate JNK and p38. Finally, our data suggest that $P2X_7$ receptor-activated microglia protect neurons against glutamate toxicity primarily because they are able to release TNF.

Key words: $P2X_7$ receptor; TNF; MAP kinase; ATP; microglia; neuroprotection

Introduction

ATP is released from damaged cells as a result of ischemia or inflammation and serves as a cell-to-cell mediator through cell surface P2 receptors, which are widely distributed throughout the nervous system (Inoue, 2002). P2 receptor subfamilies have been divided into two subtypes: P2X and P2Y. P2X receptors ($P2X_1$–$P2X_7$) are coupled to nonselective cation channels, allowing influx of Na^+ and Ca^{2+}, leading to transient cell depolarization, whereas P2Y receptors ($P2Y_1$, $P2Y_2$, $P2Y_4$, $P2Y_6$, $P2Y_{11}$, $P2Y_{12}$, $P2Y_{13}$, and $P2Y_{14}$) are G-protein coupled, and their activation leads to inositol lipid hydrolysis, intracellular Ca^{2+} mobilization, or modulation of adenylate cyclase activation (North and Surprenant, 2000; Sak and Webb, 2002). Microglia have been shown to express multiple P2 receptor subtypes, including $P2X_7$, $P2Y_2$, and $P2Y_{12}$ (Norenberg et al., 1994; James and Butt, 2002), indicating that ATP may be a critical regulator of microglial cell function. In fact, ATP strongly induces microglial chemotaxis via the G_i- and G_o-coupled $P2Y_{12}$ receptor (Honda et al., 2001) and stimulates the release of plasminogen, interleukin-6 (IL-6), and IL-1β (Ferrari et al., 1997; Inoue et al., 1998; Shigemoto-Mogami et al., 2001) by means of different types of P2 receptor and intracellular signals. ATP also stimulates the *de novo* synthesis and release of tumor necrosis factor (TNF) from rat microglia that flows from the activation of $P2X_7$ receptors, extracellular signal-regulated kinase (ERK), and p38 mitogen-activated protein (MAP) kinase (Hide et al., 2000). The precise roles of each of these MAP kinases in $P2X_7$ receptor-mediated TNF release have not yet been determined. Moreover, although the ATP-mediated activation of ERK and p38 by ATP occurs in the absence of extracellular Ca^{2+}, it is still not known precisely how MAP kinases are activated via $P2X_7$ receptors.

TNF is a proinflammatory cytokine that is upregulated in the brain in response to various insults or injury. This cytokine is mainly expressed by microglia and astrocytes around the injured area. The function of TNF, however, remains controversial.

Received Aug. 14, 2003; revised Oct. 6, 2003; accepted Oct. 7, 2003.

This work was supported by Grants-in-Aid 11670089 and 15590229 from the Ministry of Education, Science, and Culture of Japan and partly supported by the Promotion of Fundamental Studies in Health Science of the Organization for Pharmaceutical Safety and Research. We thank Dr. Peter Thatam (University College London, London, UK), Dr. Donald MacPhee (Radiation Effects Research Foundation, Hiroshima, Japan), and Masaya Tanaka for helpful comments; Yuko Kawai and Akiyo Matsubara for technical assistance; and the Research Center for Molecular Medicine (Hiroshima University School of Medicine) for the use of its facilities.

Correspondence should be addressed to Izumi Hide, Department of Pharmacology, Graduate School of Biomedical Sciences, Hiroshima University, 1-2-3 Kasumi, Minami-ku, Hiroshima 734-8551, Japan. E-mail: ihide@hiroshima-u.ac.jp.

DOI:10.1523/JNEUROSCI.3792-03.2004

 0270-6474/04/240001-07$15.00/0

Although TNF has been implicated in the acceleration of injury and the pathology of neurodegenerative diseases, recently emerging evidence suggests that TNF may also serve a protective role. The precise mechanisms involved in these two seemingly conflicting activities are still undetermined, as is the role of the TNF that is released by $P2X_7$ receptor-activated microglia.

In the present study, we investigated the signaling mechanism by which the activation of microglial $P2X_7$ receptors regulates TNF release via ERK, JNK (c-Jun N-terminal kinase), and p38 MAP kinase. We also examined whether the TNF released by microglia is toxic or protective for neurons. Our data demonstrate that ERK, JNK, and p38 contribute in different ways to the ATP-provoked production of TNF. In addition to outlining a new mechanism for the activation of JNK and p38 via the $P2X_7$–src-family protein tyrosine kinase pathway, we provide the first evidence that $P2X_7$ receptor-activated microglia protect neurons against glutamate neurotoxicity because they release TNF.

Materials and Methods

Reagents. All reagents for cell culture, ATP, and 2′–3′-*O*-(benzoylbenzoyl) ATP (BzATP) were obtained from Sigma (St. Louis, MO), and a rat TNF ELISA kit was obtained from Biosource International (Camarillo, CA). Antibody kits for p42–p44 (ERK), JNK, and p38 MAP kinase were obtained from Cell Signaling Technology (Beverly, MA). All other reagents were purchased from commercial sources and were of the highest available purity. We checked all reagents used for endotoxin contamination.

Cell culture. Microglia were obtained from primary cell culture of neonatal rat brains as described previously (Nakajima et al., 1989, 1992). After 7–16 d in culture, microglia were prepared as a floating cell suspension. Aliquots ($1.5–2.0 \times 10^5$ cells) were transferred to the wells of a 24 well plate and allowed to adhere at 37°C for 45 min. Unattached cells were removed by rinsing with serum-free DMEM. Neuron-enriched cultures were prepared from primary cell culture of neonatal rat brain cortex. For neuron–microglia cocultures, cortical neurons were seeded into 24 well plates, and microglia were transferred in Transwell coculture inserts (Costar, Cambridge, MA).

TNF assay. For the assay of TNF release, microglia were incubated with 0.4 ml of serum-free DMEM with or without drugs for 3 hr. For the assay of intracellular TNF, microglia were incubated for 2 hr and then solubilized with 0.1% Triton X-100. TNF was assayed in 50 μl samples using a rat TNF ELISA kit according to the instructions of the manufacturer.

RNA extraction. Microglia were plated in 60 mm dishes (7.5×10^5 cells per 3 ml per dish) and stimulated with ATP or the $P2X_7$ agonist BzATP for 1 hr. The cells were dissolved in Trizol LS reagents (Invitrogen, Gaithersburg, MD) before total RNA extraction. Briefly, samples were ethanol precipitated, the pellets were dissolved in RNase-free water, and RNA concentrations were determined spectrophotometrically.

Real-time reverse transcription-PCR assay. Total TNF mRNA was measured by real-time quantitative reverse transcription (RT)-PCR (ABI Prism model 7700 sequence detection system; PerkinElmer Applied Biosystems, Foster City, CA). RT-PCR was performed using the TaqMan one-step RT-PCR master mix reagents kit according to the protocol of the manufacturer (PerkinElmer Applied Biosystems). The sequences of the forward and reverse primers were 5′-ACAAGGCTGCCCCGACTAC-3′ and 5′-TCCTGGTATGAAATGGCAAACC-3′, respectively. The TaqMan fluorogenic probe was 5′-6FAM-TGCTCCTCACCCACACCGTCAGC-TAMRA-3′. During PCR amplification, 5′ nuclease activity of AmpliTaq Gold DNA polymerase cleaves the TaqMan probe, separating the 5′ reporter dye from 3′ quencher dye, resulting in increased fluorescence of the reporter. Reaction conditions for PCR were as follows: 40 cycles of amplification by denaturing to 95°C for 15 sec and extending at 60°C for 1 min. The threshold cycle, which correlates inversely with the target mRNA levels, was measured as the cycle number at which the reporter fluorescent emission increases above a threshold level. The TNF mRNA levels were corrected for glyceraldehyde-3-phosphate dehydrogenase (GAPDH) RNA using a VIC probe according to the protocol of the manufacturer.

Western blot analysis. Western blots were performed for the analysis of ERK (p44 and p42), JNK, and p38 activation using a MAP kinase antibody kit according to the protocol of the manufacturer. In brief, the cells were washed with PBS, lysed by adding SDS sample buffer, and sonicated. After heating to 95°C for 5 min, the protein samples were separated by SDS-PAGE and blotted onto polyvinylidene difluoride membranes. The membranes were blocked with blocking buffer containing 3% skim milk for 3 hr at room temperature and incubated with primary antibody with gentle agitation overnight at 4°C. After washing, the membranes were incubated for 1 hr at room temperature with horseradish peroxidase-conjugated secondary antibody and horseradish peroxidase-conjugated anti-biotin antibody to detect biotinylated protein markers. The membranes were then washed and incubated with Lumi GLO, and the proteins were detected by exposure to x-ray film.

Viability assay. The viability of neurons was assessed by a 3-[4,5-dimethylthiazol-2-yl]-2,5-diphenyltetrazolium bromide (MTT) assay on the basis of the reduction of the tetrazolium salt MTT by the mitochondrial dehydrogenase in living cells.

Statistical analysis. Student's *t* test was used in all determinations of statistical significance.

Results

The roles of ERK, JNK, and p38 MAP kinase in TNF mRNA expression and the production and release of TNF in ATP-stimulated microglia

ATP rapidly activates ERK, JNK, and p38 MAP kinase in microglia. To investigate possible roles of ERK, JNK, and p38 in ATP-induced TNF release, we examined the inhibitory effects of 10 μM 1,4-diamino-2,3-dicyano-1,4-bis[2-amino-phenylthio]-butadiene (U0126) [which inhibits MEK (mitogen-activated protein kinase kinase)], 30 μM anthra[1,9-cd]pyrazol-6(2H)-one (SP600125) (which inhibits JNK), and 15 μM 4-(4-fluorophenyl)-2-(4-methylsulfinylphenyl)-5-(4-pyridyl)IH-imidazole (SB203580) (which inhibits p38) on the release of TNF from ATP-stimulated microglia. All three inhibitors proved to be capable of reducing the amounts of TNF released by ATP-treated microglia very significantly, suggesting that TNF release is dependent on the activities of all three MAP kinases (Fig. 1*A*). To confirm the supposed selectivity of these particular inhibitors, we conducted experiments with the two additional inhibitory compounds 2-(2′-amino-3′-methoxyphenyl)-oxanaphthalen-4-one (PD98059) (which inhibits MEK) and 4-(4-fluorophenyl)-2-(4-hydroxyphenyl)-5-(4-pyridyl)IH-imidazole (SB202190) (which inhibits p38) and found that 25 μM PD98059 and 10 μM SB202190 were also capable of potently suppressing the ATP-induced release of TNF (by 57 and 60%, respectively). Next we examined the effects of three of these inhibitors (U0126, SP600125, and SB203580) on the intracellular accumulation of TNF in microglia during a 2 hr period of stimulation with ATP to determine whether all three MAP kinases are involved in the regulation of the *de novo* production of TNF. Once again, all three inhibitors markedly reduced the intracellular levels of TNF in ATP-stimulated microglia (Fig. 1*B*). These data suggest that ERK, JNK, and p38 MAP kinase are all involved in both the production and the release of TNF by ATP-treated microglia.

To determine whether all three kinases also regulate TNF transcription, we used real-time RT-PCR analysis to examine the effects of the three inhibitors on ATP-induced TNF mRNA expression. As shown in Figure 1*C*, ATP treatment led to a marked increase in TNF mRNA levels; moreover, the extent of this increase was greatly reduced in the presence of either U0126 or SP600125 but did not appear to be affected by SB203580. Thus, although all three kinases appear to be critical for ATP-induced TNF production, they appear to have different modes of action, with ERK and JNK acting to regulate transcription of the TNF

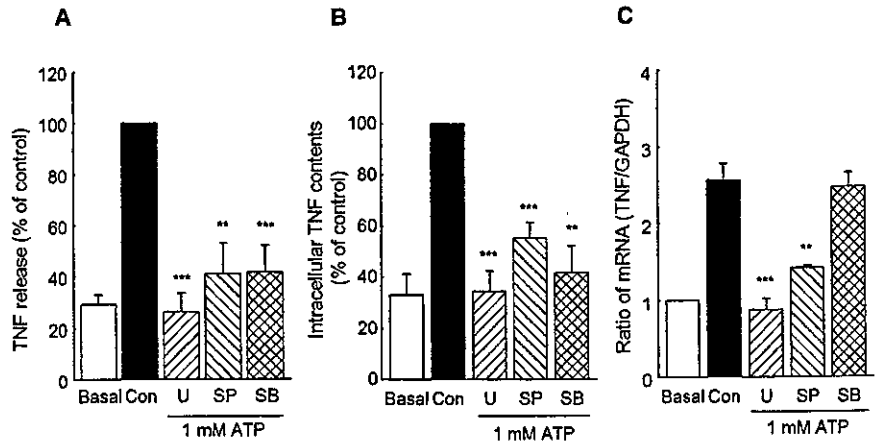

Figure 1. Effects of U0126 (U), SP600125 (SP), and SB203580 (SB) on ATP-induced TNF release, intracellular TNF production, and mRNA expression in microglia. The cells were treated with 10 μM U0126, 30 μM SP600125, or 15 μM SB203580 for 15 min and stimulated with 1 mM ATP for 3 hr (*A*), 2 hr (*B*), and 1 hr (*C*). The released TNF (*A*) and the intracellular TNF contents (*B*) were measured by ELISA. Values are expressed as mean ± SEM of percentage of release compared with ATP alone from three independent experiments. Values of 100% for the release and intracellular production of TNF in ATP-stimulated microglia were 178.8 ± 22.2 and 407.0 ± 45.6 pg/10^6 cells, respectively. *C*, The expression of TNF mRNA was quantified by real-time RT-PCR. Values are shown as the ratio of TNF mRNA versus GAPDH mRNA. Data are expressed as mean ± SEM of ratio of expression compared with ATP or BzATP alone from three independent experiments. $^{**}p < 0.01$; $^{***}p < 0.001$, significantly different from the control (Con) (*t* test).

gene and p38 only acting post-transcriptionally to interfere with the production or release of TNF.

p38 mediates the transport of TNF mRNA from the nucleus to the cytoplasm

A recent report indicates that the nucleocytoplasmic transport of TNF mRNA in lipopolysaccharide (LPS)-stimulated macrophages is regulated by ERK-dependent signals (Dumitru et al., 2000). We therefore attempted to clarify the mechanism by which p38 mediates post-transcriptional regulation of TNF production by examining the localization of TNF mRNA in the nucleus and the cytoplasm of microglia. We used Western blots of the marker proteins octamer-binding protein 1 (Oct-1) and heat shock protein 90 (Hsp-90) to confirm the efficacy of the technique used to separate the nuclear and cytoplasmic fractions (Fig. 2*B*). Our results indicated that ATP treatment led to significantly increased TNF mRNA levels in the cytoplasm as well as in the nucleus; presumably, this meant that the TNF mRNA had been exported from the nucleus to the cytoplasm so that new TNF protein molecules could then be synthesized on ribosomes (Fig. 2*A*). Interestingly, exposure of ATP-treated microglia to SB203580 did not appear to have any effect on the significantly increased levels of TNF mRNA that we observed in nuclei, but it did appear to prevent any comparable increase in cytoplasmic TNF mRNA levels from becoming evident (Fig. 2*A*). These data could be indicating that p38 has a role in regulating the nucleocytoplasmic transport of TNF mRNA in ATP-stimulated microglia, although we cannot rule out other possible explanations, including, for example, differences in the half-life of TNF mRNA in the nucleus and the cytoplasm.

$P2X_7$ receptors are coupled to JNK and p38 activation but not to ERK activation

One reason for suspecting that ATP-induced TNF release is mediated by $P2X_7$ receptors is that the optimal concentration of ATP that induces TNF release is approximately equivalent to the concentration needed to activate $P2X_7$ (i.e., of the order of 1 mM). Moreover, although we reported previously that BzATP (a $P2X_7$ agonist) is able to mimic the effects of ATP in provoking TNF release (Hide et al., 2000), we now find that α,β-methylene ATP (which is known to be a P2X receptor agonist and not a $P2X_7$ agonist) has no such effect (data not shown). We were able to confirm the involvement of $P2X_7$ receptors by showing that brilliant blue G (BBG), a $P2X_7$ receptor blocker, suppresses ATP- as well as BzATP-induced TNF release (Fig. 3*A*). We then tried to determine whether $P2X_7$ receptors are able to activate MAP kinases by examining the effects of BBG on the ATP-induced activation of ERK, JNK, and p38. The results in Figure 3*C* indicate that BBG is capable of selectively inhibiting the ATP-induced activation of JNK and p38 but appears to have little if any effect on the activation of ERK. Similar results were obtained using BzATP-stimulated cells (Fig. 3*B*,*D*). These results indicate that the activation of $P2X_7$ receptors does lead to JNK and p38 activation, and that ERK activation occurs by some other, as yet unidentified, route.

The $P2X_7$ receptor-mediated activation of JNK and p38 is protein tyrosine kinase dependent

Despite the fact that the $P2X_7$ receptor can and does function as a cation channel, activation of JNK and p38 appears to be independent of extracellular Ca^{2+} (Hide et al., 2000) and may therefore be dependent on a mechanism that is independent of Ca^{2+} influx. We therefore decided to investigate a possible involvement of PTK (protein tyrosine kinase) in this pathway by studying the effects of a general PTK inhibitor, genistein, on both TNF release and the activation of each of the MAP kinases that are induced by ATP. We found that genistein significantly inhibited the ATP-induced activation of JNK and p38 (but not that of ERK) (Fig. 4*C*) as well as the ATP-induced release of TNF, and that it did all of these things in a concentration-dependent manner (Fig. 4*A*). We obtained similar results with a second PTK inhibitor known as tyrphostin A25 (data not shown). We then found that the *src*-family PTK inhibitor PP2 also appeared to suppress ATP-induced TNF release, and that its negative control counterpart PP3 had no comparable effect (Fig. 4*B*). PP2 also appeared to inhibit the BzATP-induced activation of JNK and p38 but not that of ERK (Fig. 4*D*). Together, these findings suggest that a PTK, almost certainly a *src*-family PTK, can act downstream of the $P2X_7$ receptor to activate both JNK and p38; this could then lead to the synthesis and subsequent transport of TNF mRNA.

$P2X_7$ receptor-stimulated microglia rescue the neurons from glutamate-induced cell death by releasing TNF

Possible interactions between microglia, the TNF they produce, and neuronal tissue are still not well understood. To determine whether $P2X_7$ receptor-stimulated microglia and the TNF they release are harmful or protective to surrounding neurons, we developed a neuron–microglia coculture system in which primary cultured neurons and microglia are held in separate compartments that nonetheless allow them to exchange freely diffusible factors. A preliminary experiment then showed that even a

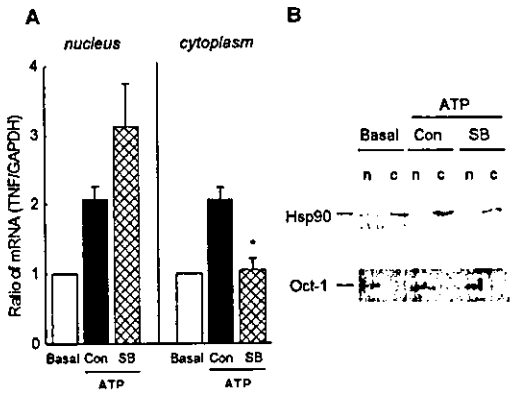

Figure 2. Distribution of TNF mRNA induced by ATP in the nucleus and cytoplasm of microglia treated with SB203580 (SB). *A*, The cells were treated with 15 μM SB203580 for 15 min and stimulated with 1 mM ATP for 1 hr. Nuclear and cytoplasmic fractions of the cells were separated by NE-PER kit, and RNA was extracted from each fraction. Values are shown as the ratio of TNF mRNA levels versus GAPDH mRNA levels. Data are expressed as mean ± SEM of ratio of expression compared with ATP alone from three independent experiments. *$p < 0.05$ significantly different from the control (Con) (*t* test). *B*, Nuclear and cytoplasmic extracts were separated by SDS-PAGE and probed with antibodies to Oct-1 [nuclear protein (n)] and Hsp-90 [cytoplasmic protein (c)] to determine the efficiency of nucleocytoplasmic separation.

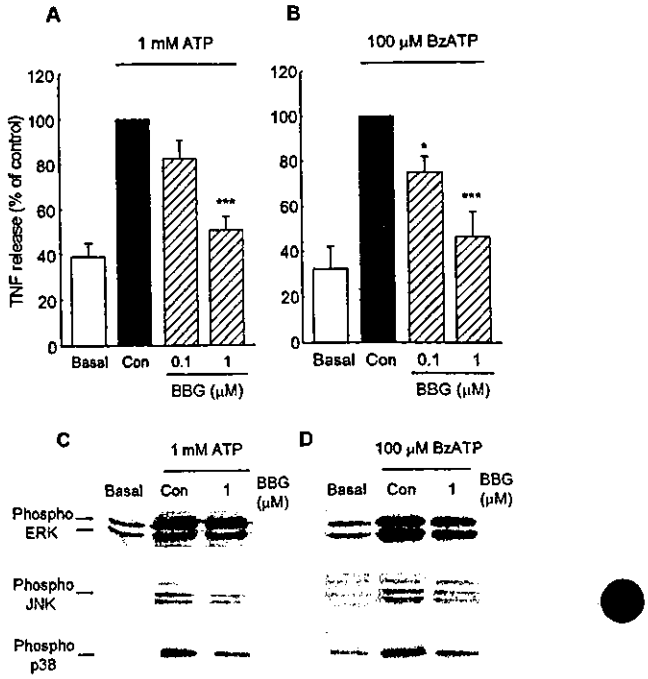

Figure 3. Effects of BBG on the release of TNF and the activation of ERK, JNK, and p38 MAP kinase in ATP- or BzATP-stimulated microglia. The cells were treated with BBG (0.1 or 1 μM) for 5 min and stimulated with 1 mM ATP (*A*, *C*) or 100 μM BzATP (*B*, *D*) for 3 hr (*A*, *B*) or 10 min (*C*, *D*). *A*, *B*, The release of TNF was measured by ELISA. Values are expressed as mean ± SEM of percentage of release compared with ATP or BzATP alone from six independent experiments. Values for 100% of release of TNF were 183.8 ± 46.3 and 350.7 ± 152.2 pg/10^6 cells in ATP- or BzATP-stimulated microglia, respectively. *$p < 0.05$; ***$p < 0.001$, significantly different from the control (Con) (*t* test). *C*, *D*, The phosphorylated (active) and total ERK, JNK, and p38 were detected by Western blotting using antibodies that recognize phosphorylated and both phosphorylated and nonphosphorylated enzymes, respectively. The levels of each total MAPK were confirmed to be identical for each lane. Similar results were obtained in at least three independent experiments.

brief (10 min) exposure of neurons to 100 μM glutamate followed by culture for 24 hr led to ~50% of them dying (Fig. 5*A*). There was no significant difference in glutamate neurotoxicity between cultures of neurons alone and neuron–microglia cocultures (Fig. 5*A*,*B*), although the neurons in cocultures that had been exposed to BzATP for 24 hr before the addition of glutamate appeared to have been given a significant level of protection against glutamate-induced cell death (Fig. 5*B*). No comparable protection was evident in neurons that were cultured on their own with BzATP (Fig. 5*A*), nor was there any evidence of a reduction in their viability (Fig. 5*A*,*B*). Interestingly, we also found that TNF-α protease inhibitor (TAPI), a well known inhibitor of TNF-α-converting enzyme (TACE), strongly inhibited the BzATP-induced release of TNF (Fig. 5*D*), and that both TACE and anti-TNF antibody significantly suppressed the protective effect that is afforded to neurons by BzATP-treated microglia (Fig. 5*C*). Furthermore, this protective effect was abolished by BBG, confirming the involvement of $P2X_7$ receptor (Fig. 5*C*). Similar results were obtained using ATP-stimulated microglia (data not shown). Together, our results strongly indicate that the neuroprotective effect of $P2X_7$ receptor-stimulated microglia stems very directly from their ability to release TNF. Whether other substances are involved remains to be seen.

Discussion

In the present study, we have shown that three MAP kinase family members (ERK, JNK, and p38) all make important contributions to the ATP-induced production of TNF in microglia, and that their precise individual roles may differ. Thus, ERK and JNK appear to regulate TNF mRNA synthesis, whereas the effects of p38 seem to be limited to the post-transcriptional level and probably involve the nucleocytoplasmic transport of TNF mRNA. Other findings led us to suggest that activation of JNK and p38 by the $P2X_7$ receptor is likely to be mediated by a *src*-family PTK. This study also revealed the biological significance of the TNF released from $P2X_7$ receptor-activated microglia.

The precise mode of action of ERK and JNK in microglial TNF production is not yet known, but it may be that they exert their effects on the promoter domain of the TNF gene by activating one of the nuclear factor-κB, nuclear factor of activated T cells, or activator protein-1 transcription factors. As the p38-mediated post-transcriptional regulation of TNF production, it is known, for example, that p38 regulates the expression of several RNA-binding proteins, which then help to stabilize TNF mRNA by interacting with the adenine uracil-rich element (ARE) region in the 3′ untranslated region of TNF mRNA (Kontoyiannis et al., 2001; Mahtani et al., 2001). Other proteins such as eukaryotic polypeptide chain initiation factor-4E, eukaryotic polypeptide chain elongation factor-1, and eukaryotic polypeptide chain releasing factor-1 also appear to contribute to translational efficiency, whereas elF-4E, a translation start factor, responds to a regulatory process downstream of p38 MAP kinase (Lee et al., 2000). Interestingly, Dumitru et al. (2000) have suggested that the transport efficacy of TNF mRNA is regulated through the ARE via ERK, although our findings suggest that p38-mediated post-transcriptional regulation of TNF production regulates the nucleocytoplasmic transport of TNF mRNA in ATP-activated microglia. Another recent paper suggested that MAP kinase-activated protein kinase 2 (MAPKAPK2), which is activated in response to direct phosphorylation by p38, also appears to be involved in the post-transcriptional regulation of TNF biosynthesis in LPS-stimulated macrophages, but it is not yet known whether MAPKAPK2 participates directly in the regulatory process (Kotlyarov et al., 1999).

Recent reports indicate that $P2X_7$ receptors are implicated in diverse cell functions, such as apoptosis, transcription, microvesicle shedding, and synaptic transmission (Humphreys et

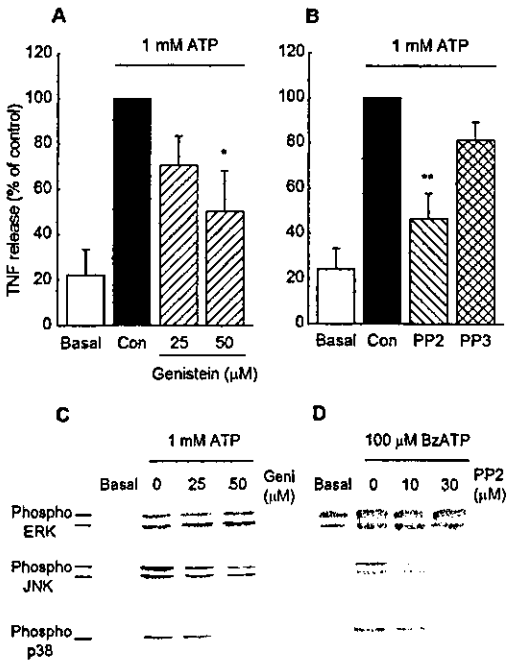

Figure 4. Effects of genistein and PP2 on the release of TNF and the activation of ERK, JNK, and p38 MAP kinase induced by ATP. Microglia were treated with genistein, a nonselective PTK inhibitor (*A*, *C*), with PP2, an *src*-family-selective PTK inhibitor, or with PP3, an inactive analog of PP2 (*B*, *D*); stimulated with 1 mM ATP or 100 μM BzATP; and then measured for the release of TNF after 3 hr (*A*, *B*) and MAP kinase activation after 10 min (*C*, *D*). Values are expressed as mean ± SEM of percentage of release compared with ATP alone from three independent experiments. Values of 100% for the release of TNF were 136.0 ± 37.0 (*A*) and 133.6 ± 65.1 (*B*) pg/10^6 cells. $^*p < 0.05$; $^{**}p < 0.01$, significantly different from the control (Con) (*t* test). *C*, *D*, The phosphorylated (Phospho) (active) and total ERK, JNK, and p38 were detected by Western blotting using antibodies that recognize either phosphorylated or both phosphorylated and unphosphorylated enzymes, respectively. The (total) levels of each MAP kinase were confirmed to be identical for each lane. Similar results were obtained in at least three independent experiments. Geni, Genistein.

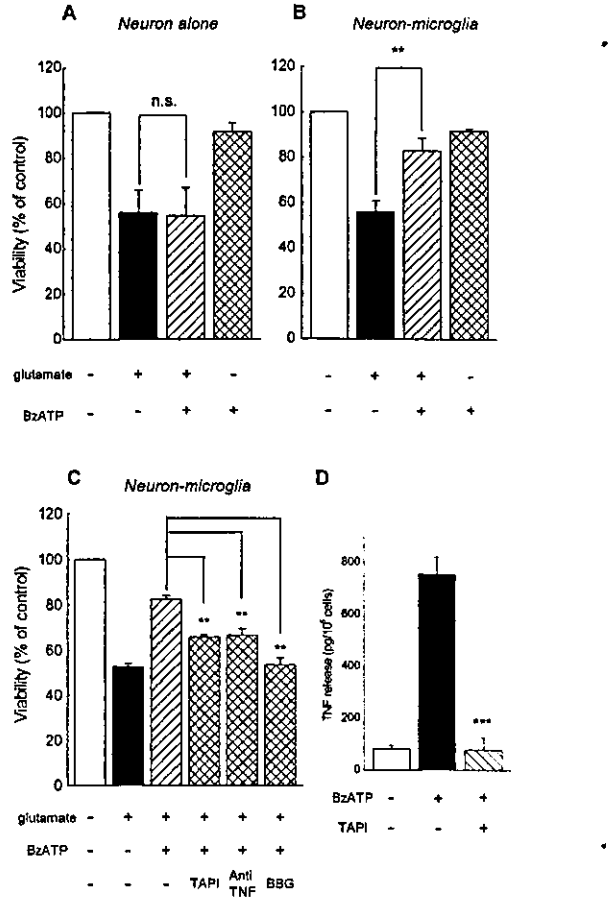

Figure 5. Effects of BzATP on the viability of primary cortical neurons in "neuron alone" cultures or neuron–microglia cocultures. Primary cultures of rat cortical neurons alone (*A*) or cocultures of neurons with microglia (*B*) were treated with 100 μM BzATP for 24 hr and then stimulated with 100 μM glutamate for 10 min. After 24 hr of incubation, neuronal cell viability was determined by MTT assay. Values are expressed as mean ± SEM of percentage of viability of control cells from three independent experiments. $^{**}p < 0.01$, significantly different from glutamate alone (*t* test). n.s., Not significant. *C*, Effects of TAPI, TACE inhibitor, anti-TNF, and BBG on BzATP-induced neuroprotection. Cortical neurons cocultured with microglia were treated with 50 μM TAPI, 10 μg/ml anti-TNF, and 1 μM BBG for 5 min before BzATP application. After 24 hr of coculture, the neurons were stimulated with 100 μM glutamate for 10 min. After 24 hr of additional incubation, neuronal cell viability was determined by MTT assay. Values are expressed as mean ± SEM of percentage of viability of control cells from three independent experiments. $^{**}p < 0.01$, significantly different from BzATP– glutamate application (*t* test). *D*, Effects of TAPI on BzATP-induced TNF release from rat microglia. $^{***}p < 0.001$.

al., 2000; MacKenzie et al., 2001; Armstrong et al., 2002), and that they have a role in the release of cytokines such as IL-1β and IL-18 (Sanz and Di Virgilio, 2000; Mehta et al., 2001). Activation of $P2X_7$ receptors may also be involved in triggering the release of TNF from rat microglia, given that: (1) a relatively high concentration of ATP (1 mM) is needed to ensure that TNF is released, (2) the $P2X_7$ agonist BzATP is much more effective as an inducer of TNF release than ATP (Hide et al., 2000), and (3) the $P2X_7$ antagonist BBG is a powerful inhibitor of ATP–BzATP-induced TNF release (Fig. 3*A*,*B*). We have also shown that BBG inhibits the activation of JNK and p38 but not ERK, thereby indicating that $P2X_7$ receptors may well be involved in the activation of JNK and p38. The $P2X_7$ receptor signaling pathways that lead up to the activation of MAP kinases still have to be properly characterized. Our data suggest that a PTK may be involved in activating JNK and p38 but not ERK. Although we do not know which PTK is involved, it may be an *src*-family tyrosine kinase such as *Lyn* or *Lck*, primarily because the *src*-family PTK-selective inhibitor PP2, but not its negative control PP3, strongly suppresses JNK and p38 activation as well as ATP-induced TNF release. As suggested recently by Denlinger et al. (2001), the Src homology 3 (SH3) domains of *src*-family kinases may well interact with the SH3 domain-binding motif in the $P2X_7$ C-terminal domain. It has also been reported that AMPA receptors, which also act as glutamate ion channel receptors, are capable of promoting glial cell line-derived neurotrophic factor release by a mechanism that is: (1) dependent on the *Lyn* tyrosine kinase and (2) independent of ion flux (Hayashi et al., 1999). ATP-induced p38 and JNK activation does not appear to be associated with Ca^{2+} influx (Hide et al., 2000; our unpublished observation), so it is conceivable that any *src*-family PTK family that plays a part in the transduction of the $P2X_7$ receptor does so because of its C-terminal domain rather than because of its ability to function as an ion channel.

$P2X_7$ receptors are believed to be involved in the activation of ERK in several cell types (Panenka et al., 2001; Budagian et al., 2003; Gendron et al., 2003). In the present study, however, activation of ERK by ATP (or even by the more powerful BzATP) was not sensitive to the $P2X_7$ antagonist BBG. Several lines of evidence point to the involvement of other P2 receptors in the activation of ERK. It has been demonstrated, for instance, that in rat primary astrocytes, ATP activates ERK via a P2Y–PKCδ–phospholipase D pathway (Neary et al., 1999), whereas the ATP re-

leased during stretch is more likely to activate ERK through $P2X_2$ and $P2Y_1$ (Neary et al., 2003). ADP and UTP also activate ERK possibly via $P2Y_{12}$ and $P2Y_2$ receptors expressed on microglia. Together, these findings lend support to the view that ERK activation may involve several non-$P2X_7$ P2 receptors. However, a recent study in which $P2X_7$ C-terminal and N-terminal mutants were expressed in human embryonic kidney 293 cells established that the N terminal of $P2X_7$ has an essential role in ERK activation and that the C terminal is required for Ca^{2+} entry (Amstrup and Novak, 2003). One possible explanation for the obvious discrepancy between these results and our findings could be that the $P2X_7$ N-terminal-associated activation signals are insensitive to BBG; unfortunately, we do not yet know whether this is the case. Nevertheless, ERK activation is clearly important for TNF-producing cells, given that it plays a key role in both the production of TNF and its subsequent release and that it does so by modulating the activity of TACE, a protein that converts 26 kDa membrane-bound pro-TNF into 17 kDa soluble TNF at the cell surface (Bezzi et al., 2001).

It is still not entirely clear whether microglia protect or harm neurons or whether TNF is beneficial or toxic (Arnett et al., 2001; Combs et al., 2001; Fontaine et al., 2002). Thus, for example, TNF appears to enhance injury, as shown by the fact that the injection of neutralizing TNF antibody into lesion sites significantly reduces experimental ischemic and traumatic injury (Barone et al., 1997; Meistrell et al., 1997). There is also recent evidence that indicates that TNF can provide protection to neurons because it is able to encourage the expression of anti-apoptotic and anti-oxidative proteins. Moreover, evidence from experiments in TNF-deficient mice indicates that although TNF has a deleterious effect during the acute response that occurs in a traumatized brain, it also has a key part to play in both the long-term behavioral recovery and the histological repair of the tissues (Scherbel et al., 1999). It is of course possible that the effects of TNF depend just as much on the postinjury time course as on its expression levels. Recent reports indicate that the dual actions of TNF are mediated via different TNF receptors, with the p55 TNF receptor 1 (TNFR1) eliciting neurotoxic effects and the p75 TNF receptor 2 (TNFR2) eliciting neuroprotection (Yang et al., 2002). Interestingly, these two receptors have been shown to have similarly specific roles in oligodendrocytes, with TNFR1 being implicated in demyelination and TNFR2 in remyelination (Arnett et al., 2001).

Given that one of our primary aims in this study was to better understand the biological significance of the TNF that is released from ATP- or BzATP-activated microglia, we decided to construct a primary neuron–microglia coculture system that could be used to screen for possible effects. Our results clearly demonstrate that BzATP-stimulated microglia provide neurons with effective protection against glutamate-induced cell death. This protective effect appears to be mediated by a soluble factor or factors released from $P2X_7$-activated microglia. One such neuroprotective factor is almost certain to be TNF, because microglia-mediated neuroprotection was suppressed in the presence of either TACE inhibitor or anti-TNF antibody. Given that ATP is likely to be released by cells that have been damaged by trauma, inflammation, or ischemia, and that low ATP concentrations can lead to chemotaxis of microglia (Honda et al., 2001), it seems not unreasonable to hypothesize that ATP can act as an emergency messenger that recruits microglia to a damaged brain area, at which point a pathway that involves ATP-activated $P2X_7$ receptors takes over and provokes the microglia to secrete neuroprotective factors such as TNF.

Here, we provided new information about the mechanisms that underlie the production of TNF via $P2X_7$ receptors and MAP kinases in rat microglia and have clearly established a neuroprotective role for the TNF that the ATP-activated microglia may go on to release. A better understanding of the mechanisms by which microglia are transformed into cells that can protect neurons, including the mechanism that leads to $P2X_7$ receptor activation, will undoubtedly help in the development of more rational approaches to the entire spectrum of neural diseases.

References

Amstrup J, Novak I (2003) $P2X_7$ receptor activates ERK1/ERK2 independent of Ca^{2+} influx. Biochem J 374:51–61.

Armstrong JN, Brust TB, Lewis RG, MacVicar BA (2002) Activation of presynaptic $P2X_7$-like receptors depresses mossy fiber-CA3 synaptic transmission through p38 mitogen-activated protein kinase. J Neurosci 22:5938–5945.

Arnett HA, Mason J, Marino M, Suzuki K, Matsushima GK, Ting JP (2001) TNFα promotes proliferation of oligodendrocyte progenitors and remyelination. Nat Neurosci 4:1116–1122.

Barone FC, Arvin B, White RF, Miller A, Webb CL, Willette RN, Lysko PG, Feuerstein GZ (1997) Tumor necrosis factor-alpha. A mediator of focal ischemic brain injury. Stroke 28:1233–1244.

Bezzi P, Domercq M, Brambilla L, Galli R, Schols D, De Clercq E, Vescovi A, Bagetta G, Kollias G, Meldolesi J, Volterra A (2001) CXCR4-activated astrocyte glutamate release via TNFα: amplification by microglia triggers neurotoxicity. Nat Neurosci 4:702–710.

Budagian V, Bulanova E, Brovko L, Orinska Z, Fayad R, Paus R, Bulfone-Paus S (2003) Signaling through $P2X_7$ receptor in human T cells involves $p56^{lck}$, MAP kinases, and transcription factors AP-1 and NF-kappa B. J Biol Chem 278:1549–1560.

Combs CK, Karlo JC, Kao SC, Landreth GE (2001) β-Amyloid stimulation of microglia and monocytes results in TNFα-dependent expression of inducible nitric oxide synthase and neuronal apoptosis. J Neurosci 21:1179–1188.

Denlinger LC, Fisette PL, Sommer JA, Watters JJ, Prabhu U, Dubyak GR, Proctor RA, Bertics PJ (2001) Cutting edge: the nucleotide receptor $P2X_7$ contains multiple protein- and lipid-interaction motifs including a potential binding site for bacterial lipopolysaccharide. J Immunol 167:1871–1876.

Dumitru CD, Ceci JD, Tsatsanis C, Kontoyiannis D, Stamatakis K, Lin JH, Patriotis C, Jenkins NA, Copeland NG, Kollias G, Tsichlis PN (2000) TNF-α induction by LPS is regulated posttranscriptionally via a Tpl2/ERK-dependent pathway. Cell 22:1071–1083.

Ferrari D, Chiozzi P, Falzoni S, Hanau S, Di Virgilio F (1997) Purinergic modulation of interleukin-1β release from microglial cells stimulated with bacterial endotoxin. J Exp Med 185:579–582.

Fontaine V, Mohand-Said S, Hanoteau N, Fuchs C, Pfizenmaier K, Eisel U (2002) Neurodegenerative and neuroprotective effects of tumor necrosis factor (TNF) in retinal ischemia: opposite roles of TNF receptor 1 and TNF receptor 2. J Neurosci 22:1–7.

Gendron FP, Neary JT, Theiss PM, Sun GY, Gonzalez FA, Weisman GA (2003) Mechanisms of $P2X_7$ receptor-mediated ERK1/2 phosphorylation in human astrocytoma cells. Am J Physiol Cell Physiol 284:C571–C581.

Hayashi T, Umemori H, Mishina M, Yamamoto T (1999) The AMPA receptor interacts with and signals through the protein tyrosine kinase Lyn. Nature 397:72–76.

Hide I, Tanaka M, Inoue A, Nakajima K, Kohsaka S, Inoue K, Nakata Y (2000) Extracellular ATP triggers tumor necrosis factor-alpha release from rat microglia. J Neurochem 75:965–972.

Honda S, Sasaki Y, Ohsawa K, Imai Y, Nakamura Y, Inoue K, Kohsaka S (2001) Extracellular ATP or ADP induce chemotaxis of cultured microglia through $G_{i/o}$-coupled P2Y receptors. J Neurosci 21:1975–1982.

Humphreys BD, Rice J, Kertesy SB, Dubyak GR (2000) Stress-activated protein kinase/JNK activation and apoptotic induction by the macrophage $P2X_7$ nucleotide receptor. J Biol Chem 275:26792–26798.

Inoue K (2002) Microglial activation by purines and pyrimidines. Glia 40:156–163.

Inoue K, Nakajima K, Morimoto T, Kikuchi Y, Koizumi S, Illes P, Kohsaka S (1998) ATP stimulation of Ca^{2+}-dependent plasminogen release from cultured microglia. Br J Pharmacol 123:1304–1310.

James G, Butt AM (2002) P2Y and P2X purinoceptor mediated Ca^{2+} sig-

nalling in glial cell pathology in the central nervous system. Eur J Pharmacol 447:247–260.

Kontoyiannis D, Kotlyarov A, Carballo E, Alexopoulou L, Blackshear PJ, Gaestel M, Davis R, Flavell R, Kollias G (2001) Interleukin-10 targets p38 MAPK to modulate ARE-dependent TNF mRNA translation and limit intestinal pathology. EMBO J 20:3760–3770.

Kotlyarov A, Neininger A, Schubert C, Eckert R, Birchmeier C, Volk HD, Gaestel M (1999) MAPKAP kinase 2 is essential for LPS-induced TNF-α biosynthesis. Nat Cell Biol 1:94–97.

Lee YB, Schrader JW, Kim SU (2000) p38 map kinase regulates TNF-α production in human astrocytes and microglia by multiple mechanisms. Cytokine 12:874–880.

MacKenzie A, Wilson HL, Kiss-Toth E, Dower SK, North RA, Surprenant A (2001) Rapid secretion of interleukin-1β by microvesicle shedding. Immunity 15:825–835.

Mahtani KR, Brook M, Dean JL, Sully G, Saklatvala J, Clark AR (2001) Mitogen-activated protein kinase p38 controls the expression and post-translational modification of tristetraprolin, a regulator of tumor necrosis factor α mRNA stability. Mol Cell Biol 21:6461–6469.

Mehta VB, Hart J, Wewers MD (2001) ATP-stimulated release of interleukin (IL)-1β and IL-18 requires priming by lipopolysaccharide and is independent of caspase-1 cleavage. J Biol Chem 276:3820–3826.

Meistrell III ME, Botchkina GI, Wang H, Di Santo E, Cockroft KM, Bloom O, Vishnubhakat JM, Ghezzi P, Tracey KJ (1997) Tumor necrosis factor is a brain damaging cytokine in cerebral ischemia. Shock 8:341–348.

Nakajima K, Hamanoue M, Shimoto M, Takei N, Kosaka S (1989) Characterization of microglia isolated from a primary culture of embryonic rat brain by a simplified method. Biomed Res 10:411–423.

Nakajima K, Shimojo M, Hamanoue M, Ishiura S, Sugita H, Kohsaka S (1992) Identification of elastase as a secretory protease from cultured rat microglia. J Neurochem 58:1401–1408.

Neary JT, Kang Y, Bu Y, Yu E, Akong K, Peters CM (1999) Mitogenic signaling by ATP/P2Y purinergic receptors in astrocytes: involvement of a calcium-independent protein kinase C, extracellular signal-regulated protein kinase pathway distinct from the phosphatidylinositol-specific phospholipase C/calcium pathway. J Neurosci 19:4211–4220.

Neary JT, Kang Y, Willoughby KA, Ellis EF (2003) Activation of extracellular signal-regulated kinase by stretch-induced injury in astrocytes involves extracellular ATP and P2 purinergic receptors. J Neurosci 23:2348–2356.

Norenberg W, Langosch JM, Gebucke-Haerter PJ, Illes P (1994) Characterization and possible function of adenosine 5′-triphosphate receptors in activated rat microglia. Br J Pharmacol 111:942–950.

North RA, Surprenant A (2000) Pharmacology of cloned P2X receptors. Annu Rev Pharmacol Toxicol 40:563–580.

Panenka W, Jijon H, Herx LM, Armstrong JN, Feighan D, Wei T, Yong VW, Ransohoff RM, MacVicar BA (2001) P2X7-like receptor activation in astrocytes increases chemokine monocyte chemoattractant protein-1 expression via mitogen-activated protein kinase. J Neurosci 15:7135–7142.

Sak K, Webb TE (2002) A retrospective of recombinant P2Y receptor subtypes and their pharmacology. Arch Biochem Biophys 397:131–136.

Sanz JM, Di Virgilio F (2000) Kinetics and mechanism of ATP-dependent IL-1β release from microglial cells. J Immunol 164:4893–4898.

Scherbel U, Raghupathi R, Nakamura M, Saatman KE, Trojanowski JQ, Neugebauer E, Marino MW, McIntosh TK (1999) Differential acute and chronic responses of tumor necrosis factor-deficient mice to experimental brain injury. Proc Natl Acad Sci USA 96:8721–8726.

Shigemoto-Mogami Y, Koizumi S, Tsuda M, Ohsawa K, Kohsaka S, Inoue K (2001) Mechanisms underlying extracellular ATP-evoked interleukin-6 release in mouse microglial cell line, MG-5. J Neurochem 78:1339–1349.

Yang L, Lindholm K, Konishi Y, Li R, Shen Y (2002) Target depletion of distinct tumor necrosis factor receptor subtypes reveals hippocampal neuron death and survival through different signal transduction pathways. J Neurosci 22:3025–3032.

ACCELERATED PUBLICATION

TIRF imaging of docking and fusion of single insulin granule motion in primary rat pancreatic β-cells: different behaviour of granule motion between normal and Goto–Kakizaki diabetic rat β-cells

Mica OHARA-IMAIZUMI, Chiyono NISHIWAKI, Toshiteru KIKUTA, Shintaro NAGAI, Yoko NAKAMICHI and Shinya NAGAMATSU[1]

Department of Biochemistry (II), Kyorin University School of Medicine, Shinkawa 6-20-2, Mitaka, Tokyo 181-8611, Japan

We imaged and analysed the motion of single insulin secretory granules near the plasma membrane in live pancreatic β-cells, from normal and diabetic Goto–Kakizaki (GK) rats, using total internal reflection fluorescence microscopy (TIRFM). In normal rat primary β-cells, the granules that were fusing during the first phase originate from previously docked granules, and those during the second phase originate from 'newcomers'. In diabetic GK rat β-cells, the number of fusion events from previously docked granules were markedly reduced, and, in contrast, the fusion from newcomers was still preserved. The dynamic change in the number of docked insulin granules showed that, in GK rat β-cells, the total number of docked insulin granules was markedly decreased to 35 % of the initial number after glucose stimulation. Immunohistochemistry with anti-insulin antibody observed by TIRFM showed that GK rat β-cells had a marked decline of endogenous insulin granules docked to the plasma membrane. Thus our results indicate that the decreased number of docked insulin granules accounts for the impaired insulin release during the first phase of insulin release in diabetic GK rat β-cells.

Key words: diabetes mellitus, exocytosis, insulin release, membrane fusion, pancreatic β-cell, total internal reflection fluorescence microscopy (TIRFM).

INTRODUCTION

Imaging techniques are powerful tools for detecting vesicle trafficking in live cells and they have provided significant advances in understanding the mechanism of exocytosis [1–3]. In particular, the use of total internal reflection fluorescence microscopy (TIRFM; also called evanescent wave microscopy), which allows fluorescence excitation within a closely restricted domain close to the plasma membrane (within 100 nm) [4], has permitted us to observe single insulin granules undergoing exocytosis. We have previously reported a new approach that uses a GFP (green fluorescent protein)-tagged insulin granule system combined with TIRFM using insulinoma MIN6 cells [5], which allowed us to observe the docking and fusion of a single insulin granule with a high degree of time resolution. Nevertheless, TIRF imaging using primary β-cells was required to examine the altered exocytosis in diabetic β-cells, because the use of an animal model of disease is essential to reveal the pathophysiology.

In Type II diabetes, the impaired insulin release in the pancreatic β-cells when stimulated by glucose is well established [6]; in particular, the β-cell defect in Type II diabetes is characterized by a lack of first-phase insulin release in response to glucose stimulation [7,8]. Although the precise molecular mechanism of insulin release has yet been determined, it is generally accepted that the ATP-sensitive K^+ channels play a central role in insulin release [9,10]. Because the electrophysiological properties of the ATP sensitivity of the ATP-sensitive K^+ channels are not altered in the β-cells in diabetic animal models [11,12], impairments of the glucose metabolism may be involved in the defect in insulin release. Indeed, there are several reports that have shown that abnormal glucose metabolism in diabetic β-cells contributes to a failure in insulin release [13–16].

On the other hand, the fundamental components of the secretory machinery required for the docking and fusion of vesicles in neuronal cells [17] are also expressed in pancreatic β-cells [18,19]. We [20] and others [21,22] have demonstrated that the expression of the insulin exocytosis machinery, such as SNARE (soluble *N*-ethylmaleimide-sensitive fusion protein attachment protein receptor) proteins, is impaired in diabetic Goto–Kakizaki (GK) rat islets. Therefore, it is conceivable that there must be impairments in the insulin exocytotic process in diabetic β-cells; however, so far there has been no direct evidence to show that the final step of insulin exocytosis is impaired in diabetic β-cells, because of the limited methodologies previously available.

In the present study, we obtained high-resolved images of primary rat β-cells using a TIRF imaging system, which allowed us to explore the impaired docking and fusion status of insulin granules in live diabetic GK rat β-cells.

EXPERIMENTAL

Cells

Diabetic GK rats and non-diabetic male Wistar rats were obtained from a commercial breeder (Oriental Yeast, Tokyo, Japan). The rats were given free access to food and water until the start of experiments, which were conducted with 10-week-old male rats. The body weight of GK rats was not statistically different from that of controls. The plasma glucose concentration in the fed state, measured by the glucose-oxidase method with a glucose analyser (Toecho Super, Kyoto Daiichi Kagaku, Kyoto, Japan), was 222 ± 14 mg/dl ($n = 16$) in GK rats and 104 ± 11 mg/dl ($n = 18$) in control rats respectively ($P < 0.0001$). Pancreatic islets of Langerhans were isolated by collagenase digestion [20], with

Abbreviations used: FBS, fetal bovine serum; GFP, green fluorescent protein; eGFP, enhanced GFP; GK, Goto–Kakizaki; KRB, Krebs–Ringer buffer; RRP, readily-releasable pool; TIRF, total internal reflection fluorescence; TIRFM, TIRF microscopy.

[1] To whom correspondence should be addressed (e-mail shinya@kyorin-u.ac.jp).

some modification. Isolated islets were dissociated into single cells by incubation in Ca^{2+}-free Krebs–Ringer buffer (KRB) containing 1 mM EGTA, and cultured on fibronectin-coated (Koken Co., Tokyo, Japan) high-refractive-index glass coverslip (Olympus) in RPMI 1640 medium (Gibco BRL), supplemented with 10 % FBS (fetal bovine serum) (Gibco BRL), 200 units/ml penicillin and 200 μg/ml streptomycin at 37 °C, in an atmosphere of 95 % air/5 % CO_2.

Constructs and expression

Insulin-eGFP (enhanced GFP) cDNA expression vector was constructed in two steps. Human pre-proinsulin cDNA pchi 1–19 (provided by Professor G. I. Bell, Department of Biochemistry and Molecular Biology, University of Chicago, Chicago, IL, U.S.A.) lacking a TGA stop codon was amplified by PCR using forward primer, 5′-*GAATTC*CGGGGGTCCTTCTGCCATG-3′ (*Eco*R1 site is italicized), and reverse primer, 5′-*GGATCC*-CAGTTGCAGTAGTTCTCCAGC-3′, where TGA was replaced by TGG. The product was subcloned into a pGEM^{T}easy vector (Promega). The approx. 0.3 kb insulin cDNA fragment lacking stop codon was cleaved by *Eco*R1 and *Bam*H1 double digestion, which was subcloned into the *Eco*R1 and *Bam*H1 site of multiple cloning sites of pEGFP-N1 (Clontech/BD Biosciences, Palo alto, CA, U.S.A.). For the recombinant adenovirus production of insulin–GFP, a cDNA fragment containing pre-proinsulin and GFP was cut by *Eco*R1 and *Not*I restriction enzymes, which was ligated into the pAdex1CA cosmid vector, and Adex1CA insulin-GFP was prepared and amplified by the standard protocol (Takara Shuzo Co., Kyoto, Japan) as described previously [23]. The reverse primer used here encodes the C-terminus of pre-proinsulin, ending LENYCNWD. The fusion with the N-terminus of eGFP includes a short linker (provided by the pEGFP-N1 plasmid) such that the sequence reads LENYCNWDPPVATM (the linker sequence is underlined and M is the first residue of eGFP). Thus the junction between the C-terminus of pre-proinsulin and eGFP is different to that used in a previously reported construct [24]; this difference may account for the differential trafficking of the two constructs. For the infection of the pancreatic β-cells with the recombinant adenovirus, cultured single cells were incubated with RPMI 1640 medium (5 % FBS) and the required adenovirus (Adex1CA insulin-GFP: 30 multiplicity of infection per cell) for 1 h at 37 °C, after which RPMI 1640 medium with 10 % FBS was added. In normal primary β-cells infected with Adex1CA insulin-GFP, GFP-tagged insulin co-localized with IAPP (islet amyloid polypeptide) (results not shown), a marker for the insulin-containing large dense core granule [5], which indicated that GFP-tagged insulin was correctly sorted into the insulin secretory granules.

TIRFM

The Olympus total internal reflection system was used with minor modifications. Light from an Ar laser (488 nm) or an He/Ne laser (543 nm) was introduced into an inverted epifluorescence microscope (IX70, Olympus) through a single-mode fibre and two illumination lenses; the light was focused at the back focal plane of a high-aperture objective lens (Apo 100 × OHR; NA 1.65, Olympus). To observe GFP, we used a 488-nm laser line for excitation and a 515-nm long-pass filter for the barrier. To observe the fluorescence image of Cy3, we used a 543-nm laser line and a long-pass 590-nm filter. The infected cells on the glass coverslip (Olympus) were mounted in an open chamber and incubated for 30 min at 37 °C in KRB containing 110 mM NaCl, 4.4 mM KCl, 1.45 mM KH_2PO_4, 1.2 mM $MgSO_4$, 2.3 mM calcium gluconate, 4.8 mM $NaHCO_3$, 2.2 mM glucose, 10 mM Hepes (pH 7.4) and 0.3 % BSA. Cells were then transferred onto the thermostat-controlled stage (37 °C). Stimulation with glucose was achieved by addition of 52 mM glucose/KRB into the chamber (final glucose concentration, 22 mM). Diodomethane sulphur immersion oil (Cargille Laboratories) was used to make contact between the objective lens and the coverslip. Measured penetration depths at $\theta = 61.3°$ was about 80 nm [5].

Acquiring the images and analysis

Images were collected by a cooled charge-coupled-device camera (Micromax, MMX-512-BFT, Princeton Instruments; operated with Metamorph 4.6, Universal Imaging). Images were acquired every 50 ms. Most analyses, including tracking (the single projection of different images) and area calculations, were performed using Metamorph software. To analyse the data, fusion events were manually selected, and the average fluorescence intensity of individual granules in a 1 μm × 1 μm square placed over the granule centre was calculated. The number of fusion events was manually counted while looping 15 000 frame time-lapses. Sequences were exported as single TIFF files and further processed using Adobe Photoshop 6.0 or they were converted into QuickTime movies.

Immunohistochemical analysis

Cells were fixed, made permeable with 2 % paraformaldehyde/0.1 % Triton X-100, and processed for immunocytochemistry as described previously [23]. Cells were labelled with monoclonal anti-insulin antibodies (Sigma), then processed with Cy3-conjugated anti-mouse IgG antibody (Amersham Pharmacia Biotech). Immunofluorescence staining was detected with TIRFM.

RESULTS

TIRF imaging analysis of single insulin granules undergoing exocytosis in normal rat primary pancreatic β-cells

Figure 1(A) shows the real-time TIRF images of a single insulin granule motion when stimulated by 22 mM glucose for 15 min in normal rat primary pancreatic β-cells (see Supplemental Movie 1, http://www.BiochemJ.org/bj/381/bj3810013add.htm). The sequential images of single granules obtained every 50 ms revealed a marked difference in exocytotic pathways between the first (0–4 min) and second phase (> 4 min). During the first phase, within the first 240 s after the addition of 22 mM glucose, the fusing granules originated mostly from morphologically previously docked granules, the so-called 'residents' that were visible before glucose stimulation (Figure 1A, resident). As shown in the sequential images of single granules, the fluorescent spot remained nearly constant, as if it were docked to the plasma membrane, then suddenly brightened and vanished within 300 ms. The fusing granules during the second phase arose from 'newcomers', which had been absent or only dimly visible before stimulation, but which probably pre-existed in a reserve pool (Figure 1A, newcomer). It is quite interesting that the newcomer was fused immediately after it reached the plasma membrane. The time from landing to fusion was less than 50 ms.

We then measured the dynamic changes in the number of insulin granules docked to the plasma membrane during the time course of glucose stimulation. The number of previously docked granules decreased, because fusion occurs in previously docked granules during the first phase (Figure 1C, dark grey line), whereas newly recruited granules docked and remained on the cell surface (Figure 1C, light grey line); as a result, the total number of

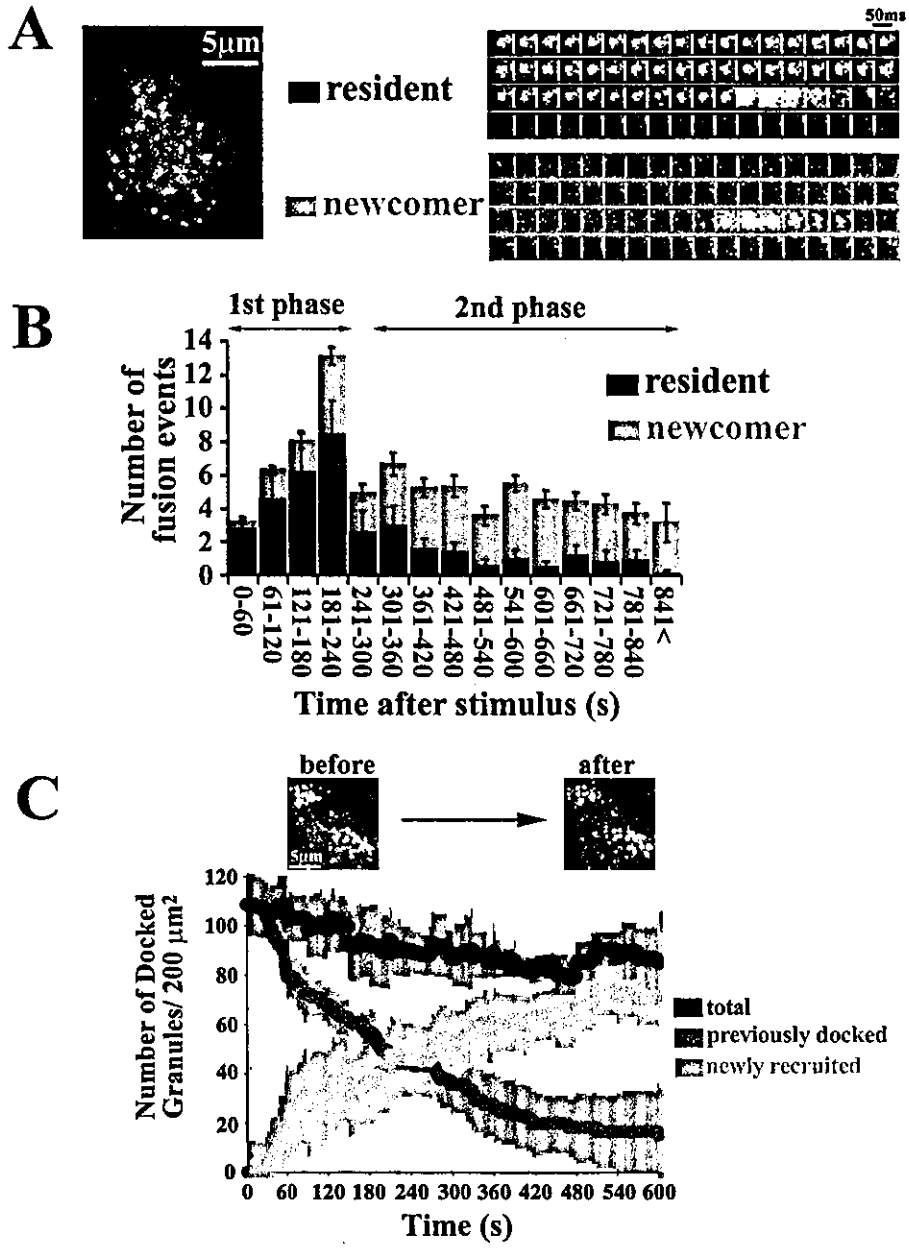

Figure 1 TIRF images and analysis of single GFP-labelled insulin granule motion in normal rat primary β-cells during glucose-induced biphasic insulin release

(**A**) The real-time motion of GFP-labelled insulin granules was imaged close to the plasma membrane (50-ms intervals) (see Supplemental Movie 1, http://www.BiochemJ.org/bj/381/bj3810013add.htm). Sequential images (1 μm × 1 μm) of a granule docking and fusing with the plasma membrane were presented during stimulation with 22 mM glucose. 'Resident' indicates that the morphologically previously docked granule is fused with the plasma membrane. Fusion is observed as the rapid spread of brightened fluorescence, followed by its disappearance. 'Newcomer' indicates that the granules approach from the inside (being absent before stimulation with 22 mM glucose), reach the plasmalemma and then are quickly fused. (**B**) Histogram showing the number of fusion events (per 200 μm^2) at 60-s intervals after stimulation ($n = 10$ cells). The black columns show the fusion from residents, and the grey columns shows that from newcomers. During the first phase, fusion occurs mostly from residents. The fusing granules during the second phase originate mostly from newcomers. (**C**) Time-dependent change of the number of insulin granules docked to the plasma membrane during glucose stimulation. The number of previously docked granules (dark grey line) and that of newly recruited granules (light grey line) during glucose-stimulation were determined by counting the granules on each sequential image. The black line represents the total number of granules docked to the plasma membrane, which corresponds to the sum of dark and light grey lines in the time course. Time 0 indicate the addition of 22 mM glucose, and the number of docked granules is presented per 200 μm^2.

docked granules, which is the sum of previously docked granules and newly recruited granules (Figure 1C, black line), was only slightly decreased to approx. 80% of the level before glucose stimulation. This finding was apparently different from results in insulinoma MIN6 cells, in which the total number of docked granules increased up to 140% of the initial number after 15 min of glucose stimulation [5].

Docking and fusion of insulin secretory granules in diabetic GK rat β-cells

The docking and fusion process of GFP-tagged insulin granules were imaged in diabetic GK rat β-cells. TIRF images revealed that the fusion from previously docked granules with 22 mM glucose stimulation was rarely observed during the first phase

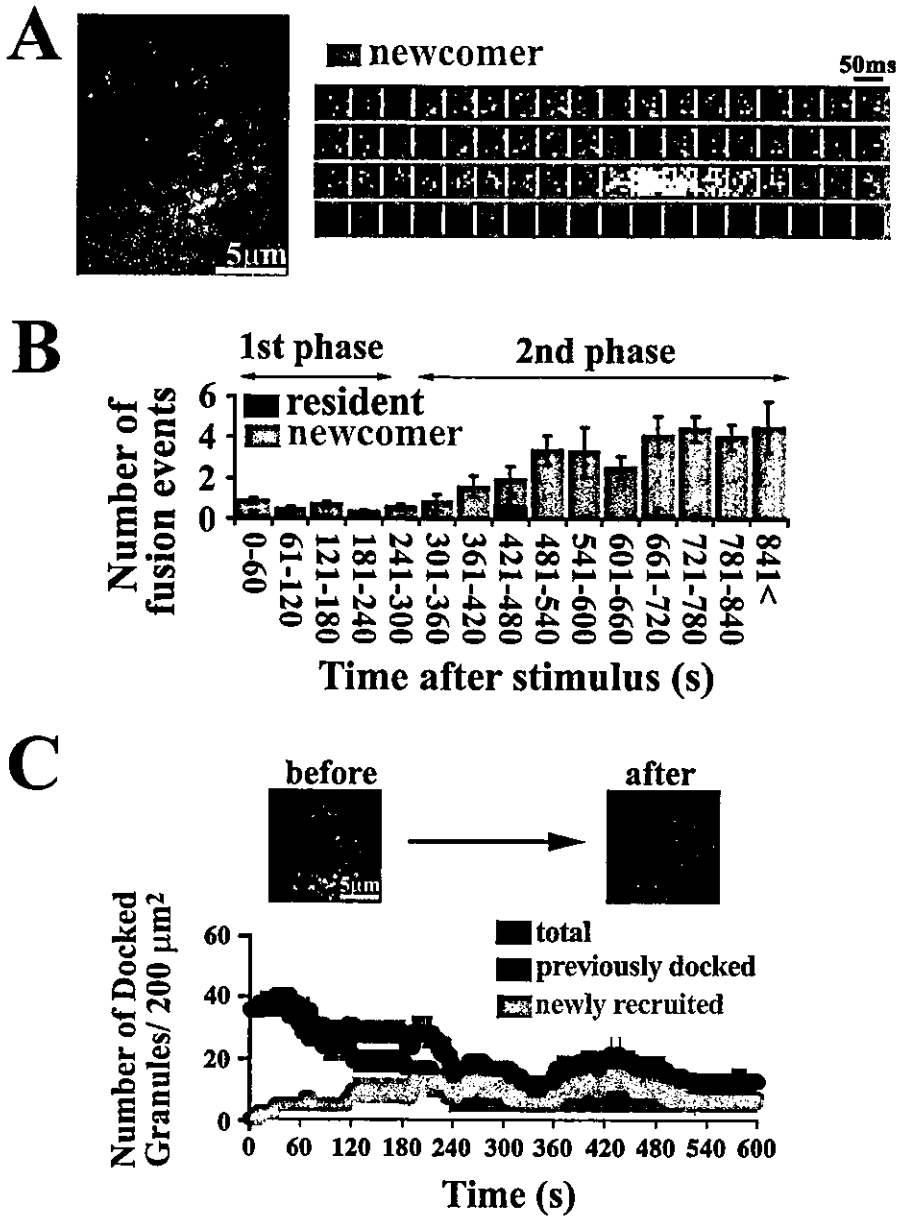

Figure 2 TIRF images and analysis in diabetic β-cells prepared from GK rat pancreas

(**A**) TIRF image during glucose stimulation (see Supplemental Movie 2, http://www.BiochemJ.org/bj/381/bj3810013add.htm) and sequential images of a granule docking and fusing during the second phase. (**B**) Histogram of the number of fusion events (per 200 μm^2) in diabetic β-cells at 60-s intervals after stimulation ($n = 10$ cells). The black and grey columns represent the fusion from residents and newcomers respectively. (**C**) Time-dependent change of the number of docked granules. A line graph shows the dynamic change of docked granules in diabetic β-cells during glucose stimulation as outlined above ($n = 10$ cells).

(see Supplemental Movie 2, http://www.BiochemJ.org/bj/381/bj3810013add.htm), although there were still some previously docked granules observed at the plasma membrane (Figure 2A). The number of fusion events (2.4 ± 0.8 in 0–4 min) during the first phase was markedly reduced in diabetic GK rat β-cells (Figure 2B) compared with that (30.7 ± 2.2 in 0–4 min) in normal β-cells (Figure 1B). On the other hand, no marked differences were observed between normal and diabetic β-cells in the number of fusion events, in particular, during the later second phase (normal, 20.2 ± 1.3 in 10–16 min; diabetic, 19.5 ± 1.2 in 10–16 min). As shown in Figure 2(B), in GK rat β-cells, there was a marked reduction in the fusion from previously docked granules, and, in contrast, fusion from newcomer was almost intact, although the number of fusion events from newcomers slightly decreased. The sequential images of a single insulin granule during the second phase showed that there was not different from that observed in normal β-cells (Figure 2A, right-hand panel).

We then analysed the dynamic changes in the total number of docked granules during glucose stimulation using these TIRF images. In GK rat β-cells, the initial number of GFP-labelled docked insulin granules before glucose stimulation was already reduced (35.7 ± 2.4 versus 108.4 ± 12.9, GK β-cells versus normal β-cells; $P < 0.0001$, $n = 10$ cells). The total number of docked granules in the time course during glucose stimulation remained low, because there was no appreciable number of newly recruited granules to eventually dock to the cell surface and there was

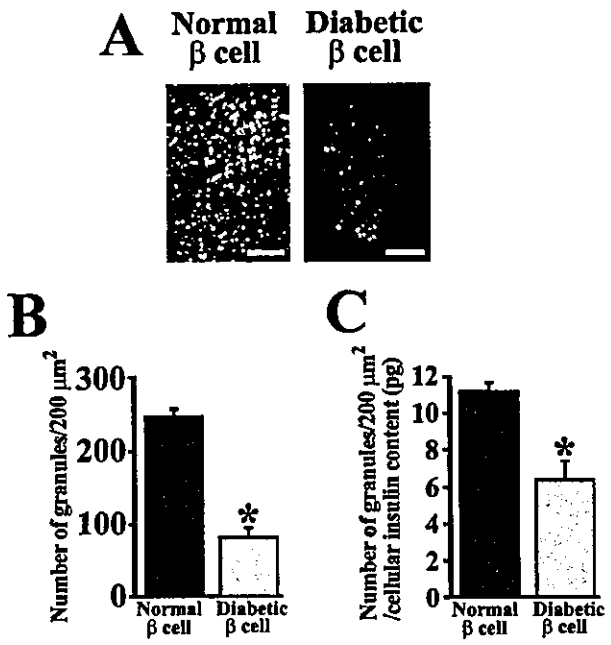

Figure 3 Histochemical study of insulin granules docked to the plasma membrane in normal and diabetic β-cells

(**A**) Endogenous insulin granules in normal and diabetic β-cells imaged by TIRF microscopy. Cells were fixed with paraformaldehyde and then immunostained for insulin. The scale bars represent 5 μm. (**B**) The number of insulin granules morphologically docked to the plasma membrane (per 200 μm^2) in normal and diabetic β-cells by TIRF images ($n = 12$ cells). (**C**) The number of docked granules normalized using cellular insulin content (12.6 ± 2.6 versus 21.7 ± 2.6 pg/cell, GK rat β-cell versus normal cell). The total insulin content in each cell was derived from the total amount of insulin in cultured cells assayed by ELISA, divided by the number of cells and used to normalize the counts. *$P < 0.0001$ compared with normal β-cells.

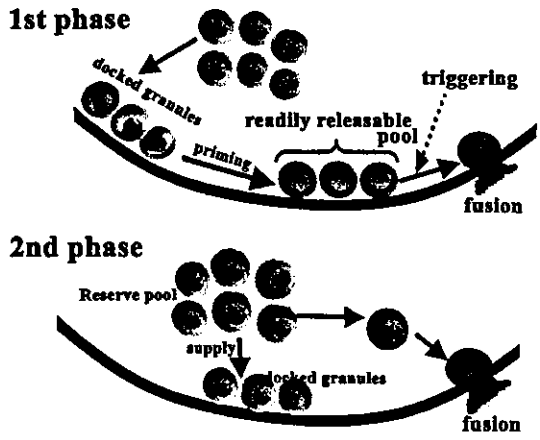

Figure 4 Proposed model for biphasic insulin exocytosis mechanism

During the first phase, some of the previously docked granules are primed by an unknown mechanism and form the RRP. The rise in intracellular [Ca^{2+}] evokes the fusion events from granules in such a pool. During the second phase, the granules jump directly from the reserve pool to the fusion site on the plasma membrane without approaching the RRP and are quickly fused.

an impairment in the cell's ability to retain the already docked granules on the cell surface (Figure 2C). As a result, the total number of docked granules decreased to 35% of initial number after 15 min of glucose stimulation. The finding that fusion from previously docked granules is severely impaired, even though that of newcomers originating from inside the granule pool is still preserved, supports our hypothesis that the insulin exocytotic pathway during the second phase is different from that during the first phase.

Decreased number of endogenous docked insulin granules in diabetic GK rat β-cells observed by TIRFM

Because granules that were fusing mostly originated from previously docked granules during the first phase (Figure 1A), we thought that the total number of endogenous insulin granules docked to the cell surface must decrease in GK β-cells. Therefore we counted the number of docked insulin granules using TIRFM in normal and diabetic β-cells by immunostaining with anti-insulin antibody. Although observing the immunostained insulin granules by epifluorescence microscopy did not allow us to count the individual granules (results not shown), TIRF imaging clearly depicted the single insulin granules morphologically docked to the plasma membrane (Figure 3A), and thus we could count the number of docked insulin granules. As expected, the GK rat β-cells showed a marked decline in the number of docked insulin granules to 33% of normal levels (81 ± 13 granules per 200 μm^2 versus 246 ± 11 per 200 μm^2; $P < 0.0001$, $n = 12$ cells) (Figure 3B). In order to exclude the possibility that this reduction is related to the insulin expression levels, the number of granules was normalized using cellular insulin content (12.6 ± 2.6 versus 21.7 ± 2.6 pg/cell, GK β-cell versus normal cell). The results demonstrated that the number of docked granules was also decreased in GK rat β-cells to 57% of normal levels (Figure 3C), suggesting that this reduction of docked granules was not related to the level of insulin expression.

DISCUSSION

TIRF images of a single insulin granule motion in normal primary β-cells showed that there was a difference in the behaviour of insulin granule motion between insulinoma MIN6 cells and primary pancreatic β-cells. In primary pancreatic β-cells the newcomer was fused immediately after it reached the plasmalemma. In insulinoma MIN6 cells, newcomers remained on the plasma membrane for 66 ± 13 s prior to fusion [5]. Furthermore, there was a distinct difference in the change of the total number of docked granules during glucose stimulation. Thus the dynamics of insulin granule motion near the plasma membrane in primary β-cells is not exactly same as that observed in insulinoma MIN6 cells. The present results in primary β-cells provide new insight into the biphasic insulin exocytotic mechanism: during the second phase, granules from the reserve pool are directly fused without approaching the RRP (readily-releasable pool), and the exocytotic pathway during the second phase does not take the same route of exocytosis as that seen during the first phase (Figure 4).

We analysed the docking and fusion of insulin granules in diabetic GK rat β-cells. Our results demonstrated that in GK rat β-cells: (1) fusion from previously docked granules was almost abolished during first phase, (2) the supply and the ability to retain the granules on the cell surface were impaired, and (3) the number of docked insulin granules decreased, which suggested that the impaired docking followed by fusion plays a role in a loss of insulin exocytosis during the first phase.

It is of interest that the number of docked insulin granules was markedly decreased in diabetic GK rat β-cells to approx. 30% of normal levels. This reduction of docked insulin granules was not due to a decreased insulin content in diabetic β-cells (Figure 3C).

Thus the decrease of docked insulin granules in GK rat β-cell may be one of factors to cause the reduced fusion events during the first phase of insulin release. However, the decreased number of fusion events appears not always to be proportional to the decrease in the number of docked granules, because few fusions were observed during the first phase, despite there being a number of docked granules remaining on the cell surface. This observation suggests that a reduction in fusion events results from not only the decreased number of docked granules, but also probably from impairments to the priming step [25] from docking to fusion; in other words, the process of unprimed docked granules becoming primed docked granules (RRP) or that from RRP to fusion must be disturbed in diabetic β-cells.

In conclusion, we present direct evidence that there is an impaired docking and fusion of insulin granules in diabetic β-cells, which contributes to the loss of first-phase insulin release.

We thank Dr I. Saito (Laboratory of Molecular Genetics, Institute of Medical Science, University of Tokyo, Japan) for the gift of adenovirus cosmid vector and parental virus. This work was supported by Grants-in-Aid for Scientific Research (C) 14570130 (to M. O.-I.), (B) 15390108 (to S. N.), Scientific Research on Priority Areas 16044240 (to M. O.-I.), and Exploratory Research 14657043 (to S.N.) from the Japanese Ministry of Education, Culture, Sports, Science and Technology, and by a grant from Japan Private School Promotion Foundation (to S. N.).

REFERENCES

1 Lang, T., Wacker, I., Steyer, J., Kaether, C., Wunderlich, I., Soldati, T., Gerdes, H. H. and Almers, W. (1997) Ca^{2+}-triggered peptide secretion in single cells imaged with green fluorescent protein and evanescent wave microscopy. Neuron **18**, 857–863
2 Rohrbach, A. (2000) Observing secretory granules with a multi-angle evanescent wave microscopy. Biophys. J. **78**, 2641–2654
3 Johns, L. M., Levitan, E. S., Shelden, E. A., Holz, R. W. and Axelrod, D. (2001) Restriction of secretory granule motion near the plasma membrane of chromaffin cells. J. Cell Biol. **183**, 177–190
4 Axelrod, D. (2001) Total internal reflection fluorescent microscopy in cell biology. Traffic **2**, 764–774
5 Ohara-Imaizumi, M., Nakamichi, Y., Tanaka, T., Ishida, H. and Nagamatsu, S. (2002) Imaging exocytosis of single insulin secretory granules with evanescent wave microscopy. J. Biol. Chem. **277**, 3805–3808
6 Efendic, S. and Ostenson, C.-G. (1993) Hormonal responses and future treatment in non-insulin-dependent diabetes mellitus. J. Intern. Med. **234**, 127–138
7 Ward, W. K., Bolgiano, D. C., McKnight, B., Halter, J. B. and Porte, Jr, D. (1984) Diminished β-cell secretory capacity in patients with non-insulin-dependent diabetes mellitus. J. Clin. Invest. **74**, 1318–1328
8 O'Rahilly, S. P., Nugent, Z., Rudenski, A. S., Hosker, J. P., Burnett, M. A., Darling, P. and Turner, R. C. (1986) Beta-cell dysfunction rather than insulin insensitivity is the primary defect in familial type 2 diabetics. Lancet **11**, 360–364
9 Ashcroft, F. and Rorsman P. (1989) Electrophysiology of the pancreatic β cell. Prog. Biophys. Mol. Biol. **54**, 87–143
10 Wollheim, C. B., Lang, J. and Regazzi, R. (1996) The exocytotic process of insulin secretion and its regulation by Ca^{2+} and G-proteins. Diabetes Rev. **4**, 276–297
11 Hughes, S. J., Faehling, M., Thorneley, C. W., Proks, P., Ashcroft, F. M. and Smith, P. A. (1998) Electrophysiological and metabolic characterization of single beta-cells and islets from diabetic GK rats. Diabetes **47**, 73–81
12 Kato, S., Ishida, H., Tsuura, Y., Tsuji, K., Nishimura, M., Horie, M., Taminato, T., Ikehara, S., Okada, H., Ikeda, H., Okada, Y. and Seino, Y. (1996) Alterations in basal and glucose stimulated voltage-dependent calcium channel activities in pancreatic beta cells of NIDDM GK rats. J. Clin. Invest. **97**, 2417–2425
13 Portha, B., Giroix, M. H., Serradas, P., Welsh, N., Hellerstrom, C., Sener, A. and Malaisse, W. J. (1988) Insulin production and glucose metabolism in isolated pancreatic islets of rats with NIDDM. Diabetes **37**, 1226–1233
14 Ostenson, C. G., Khan, A., Abdel-Halim, S. M., Guenifi, A., Suzuki, K., Goto, Y. and Efendic, S. (1993) Abnormal insulin secretion and glucose metabolism in pancreatic islets from the spontaneously diabetic GK rat. Diabetologia **36**, 3–8
15 Giroix, M. H., Vesco, L. and Portha, B. (1993) Functional and metabolic perturbations in isolated pancreatic islets from the GK rat, a genetic model of non-insulin-dependent diabetes. Endocrinology **132**, 815–822
16 Zong-Chao, L., Efendic, S., Wibom, R., Abdel-Halim, S. M., Ostenson, C. G., Landau, B. R. and Khan, A. (1998) Glucose metabolism in Goto–Kakizaki rat islets. Endocrinology **139**, 2670–2675
17 Sudhof, T. C. (1995) The synaptic vesicle cycle: a cascade of protein–protein interactions. Nature (London) **375**, 645–653
18 Nagamatsu, S., Fujiwara, T., Nakamichi, Y., Watanabe, T., Katahira, H., Sawa, H. and Akagawa, K. (1996) Expression and functional role of syntaxin 1/HPC-1 in pancreatic β cells. J. Biol. Chem. **271**, 1160–1165
19 Wheeler, M. B., Sheu, L., Ghai, M., Bouquillon, A., Grondin, G., Weller, U., Beaudoin, A. R., Bennett, M. K., Trimble, W. S. and Gaisano, H. Y. (1996) Characterization of SNARE protein expression in β cell lines and pancreatic islets. Endocrinology **137**, 1340–1348
20 Nagamatsu, S., Nakamichi, Y., Yamamura, C., Matsushima, S., Watanabe, T., Ozawa, S., Furukawa, H. and Ishida, H. (1999) Decreased expression of t-SNARE, syntaxin 1, and SNAP-25 in pancreatic beta-cells is involved in impaired insulin secretion from diabetic GK rat islets: restoration of decreased t-SNARE proteins improves impaired insulin secretion. Diabetes **48**, 2367–2373
21 Gaisano, H. Y., Ostenson, C. G., Sheu, L., Wheeler, M. B. and Efendic, S. (2002) Abnormal expression of pancreatic islet exocytotic soluble *N*-ethylmaleimide-sensitive factor attachment protein receptors in Goto–Kakizaki rats is partially restored by phlorizin treatment and accentuated by high glucose treatment. Endocrinology **143**, 4218–4226
22 Zhang, W., Khan, A., Ostenson, C. G., Berggren, P. O., Efendic, S. and Meister, B. (2002) Down-regulated expression of exocytotic proteins in pancreatic islets of diabetic GK rats. Biochem. Biophys. Res. Commun. **291**, 1038–1044
23 Nagamatsu, S., Watanabe, T., Nakamichi, Y., Yamamura, C., Tsuzuki, K. and Matsushima, S. (1999) α-Soluble *N*-ethylmaleimide-sensitive factor attachment protein is expressed in pancreatic β-cells and functions in insulin, but not γ-amino butyric acid secretion. J. Biol. Chem. **274**, 8053–8060
24 Pouli, A. E., Kennedy, H. J., Schofield, J. G. and Rutter, G. A. (1998) Insulin targeting to the regulated secretory pathway after fusion with green fluorescent protein and firefly luciferase. Biochem. J. **331**, 669–675
25 Eliasson, L., Renstrom, E., Ding, W. G., Proks, P. and Rorsman, P. (1997) Rapid ATP-dependent priming of secretory granules precedes Ca^{2+}-induced exocytosis in mouse pancreatic β-cells. J. Physiol. (London) **503**, 399–412

Received 16 March 2004/4 May 2004; accepted 5 May 2004
Published as BJ Immediate Publication 6 May 2004, DOI 10.1042/BJ20040434

THE JOURNAL OF BIOLOGICAL CHEMISTRY
© 2004 by The American Society for Biochemistry and Molecular Biology, Inc.

Vol. 279, No. 21, Issue of May 21, pp. 22532–22538, 2004
Printed in U.S.A.

Rab27 Effector Granuphilin Promotes the Plasma Membrane Targeting of Insulin Granules via Interaction with Syntaxin 1a*

Received for publication, January 20, 2004, and in revised form, March 11, 2004
Published, JBC Papers in Press, March 17, 2004, DOI 10.1074/jbc.M400600200

Seiji Torii‡, Toshiyuki Takeuchi‡, Shinya Nagamatsu§, and Tetsuro Izumi¶‖

From the ‡Laboratory of Gene Analysis and ¶Laboratory of Gene Engineering, Institute for Molecular and Cellular Regulation, Gunma University, Maebashi, Gunma 371-8512, Japan and §Department of Biochemistry, Kyorin University School of Medicine, Mitaka, Tokyo 181-8611, Japan

Secretory vesicle exocytosis is a highly regulated process involving vesicle targeting, priming, and membrane fusion. Rabs and SNAREs play a central role in executing these processes. We have shown recently that Rab27a and its effector, granuphilin, are involved in the exocytosis of insulin-containing secretory granules through a direct interaction with the plasma membrane syntaxin 1a in pancreatic beta cells. Here, we demonstrate that fluorescence-labeled insulin granules are peripherally accumulated in cells overexpressing granuphilin. The peripheral location of granules is well overlapped with both localizations of granuphilin and syntaxin 1a. The plasma membrane targeting of secretory granules is promoted by wild-type granuphilin but not by granuphilin mutants that are defective in binding to either Rab27a or syntaxin 1a. Granuphilin directly binds to the H3 domain of syntaxin 1a containing its SNARE motif. Moreover, introduction of the H3 domain into beta cells induces a dissociation of the native granuphilin-syntaxin complex and a marked reduction of newly docked granules. These results indicate that granuphilin plays a role in tethering insulin granules to the plasma membrane by an interaction with both Rab27a and syntaxin 1a. The complex formation of these three proteins may contribute to the specificity of the targeting process during the exocytosis of insulin granules.

Intracellular fusion of vesicles or organelles with their target membranes is a common reaction of the compartmental structure of eukaryotic cells that is mediated by dynamic molecular assemblies involving conserved protein families. Central to these reactions are Rab GTPase and soluble *N*-ethylmaleimide-sensitive factor attachment protein receptors (SNAREs),[1] which are conserved from yeast to man (1). The membrane-anchoring SNAREs form a four-helix bundle in a ternary protein complex that is thought to drive a fusion reaction. By contrast, many Rabs act on a more upstream process in the initial physical contact between a vesicle and its target (2). This process, known as tethering or docking, may provide specificity to membrane fusion.

Both yeast and mammalian systems have revealed various tethering factors. Some of them are large multisubunit complexes and others are long coiled-coil proteins (3). The former include the exocyst (the Sec6/8 complex), the conserved oligomeric Golgi complex (the Sec34/35 complex), the transport protein particle complexes (TRAPP-I and -II), and the Class C Vps complex (the homotypic fusion and vacuole protein sorting complex), and the latter are represented by p115 (yeast Uso1p) and EEA1. The monomeric tethering factor directly binds to Rab and functions as an effector protein, whereas the large complexes are associated with events upstream or downstream of the Rab function. These tethering factors are commonly expressed in almost all cells and function in constitutive processes depending on the accumulation of cargo. Compared with these pathways, the regulated secretory pathways that have developed in neuroendocrine cells have a unique property, which is first to store specific cargo and then to release it only in the presence of secretagogues. Because fusion frequencies and vesicle demands continuously change as a function of the external stimuli in regulated secretory pathways, releasable vesicles must be replenished in concert with fusion events. Therefore, the tethering process in regulated secretory pathways needs additional regulation compared with that in other pathways.

As in neurons, pancreatic beta cells express many components of secretory machinery, including Rab3 and its effector RIM, the SNAREs (synaptobrevin2, synaptosomal-associated protein 25, and syntaxin 1a), and SNARE-associated proteins (Munc13-1 and Munc18-1) (4, 5). They appear to function in the exocytosis of insulin-containing secretory granules, although the precise mechanism still is unclear. Although the central fusion players are shared in endocrine cells and neurons, proteins expressed in a specific cell need to be characterized. This is because each regulated secretory pathway, depending on the function of the specific cargo, has developed unique organelles in which the morphological appearance, release kinetics, and biogenesis are distinct. For example, synaptic vesicles in neurons are placed at the active zone opposite the synaptic cleft and undergo rapid cycles of exocytosis and endocytosis at the nerve termini. Vesicle recycling does not require input from the biosynthetic pathway because the neurotransmitter is refilled by specific transporters on the vesicle membrane. By contrast, secretory granules in endocrine cells are exocytosed with a slower onset but for a longer duration and rely on *de novo*

* This work was supported by grants-in-aid for scientific research on priority areas (to T. I.) and for young scientists (to S. T.) and a grant of the 21st Century Center of Excellence program from the Ministry of Education, Culture, Sports, Science, and Technology of Japan. It also was supported in part by grants from the Takeda Science Foundation and The Naito Foundation and by a Japan Insulin Study Group Award (to T. I.). The costs of publication of this article were defrayed in part by the payment of page charges. This article must therefore be hereby marked "*advertisement*" in accordance with 18 U.S.C. Section 1734 solely to indicate this fact.

‖ To whom correspondence should be addressed: Dept. of Molecular Medicine, Institute for Molecular and Cellular Regulation, Gunma University, 3-39-15, Showa-machi, Maebashi, Gunma 371-8512, Japan. Tel.: 81-27-220-8856; Fax: 81-27-220-8860; E-mail: tizumi@showa.gunma-u.ac.jp.

[1] The abbreviations used are: SNARE, soluble *N*-ethylmaleimide-sensitive factor attachment protein receptor; EGFP, enhanced green fluorescent protein; ACTH, adrenocorticotropic hormone; HA, hemagglutinin; Cy3, indocarbocyanine; GST, glutathione *S*-transferase; SgIII, secretogranin III.

synthesis of polypeptides in the endoplasmic reticulum and transport through the Golgi network to the plasma membrane, although they have no discrete docking sites. Even among secretory granules in endocrine cells, there are some differences in exocytotic characteristics. For instance, pancreatic beta cells contain a small number of insulin granules that are docked below the plasma membrane, whereas chromaffin cells contain a large number of morphologically docked vesicles (6–8). Thus, the tethering process in regulated secretory pathways likely is diverse.

From the analysis of genes preferentially expressed in pancreatic beta cells, we have identified previously a novel set of Rab and its effector, Rab27a and granuphilin, respectively, both of which are specifically localized on insulin-containing mature granules (9, 10). Overexpression of Rab27a in beta cells enhanced depolarization-induced insulin secretion without affecting basal secretion, suggesting that granules in a pool primed for fusion are accumulated by the action of Rab27a. Granuphilin directly binds to the plasma membrane-anchored SNARE, syntaxin 1a, and Rab27a regulates this interaction (11). Our data, estimated by the universal function of Rab effectors, suggest that granuphilin has a function in tethering insulin granules with the plasma membrane at the docking stage of exocytosis. In the present study, we provide both morphological and biochemical evidence that granuphilin efficiently induces the translocation of granules to the plasma membrane. The tethering function of granuphilin requires its interaction with both Rab27a and syntaxin 1a. We propose that granuphilin regulates accurate targeting of insulin granules to the exocytotic site by a specific interaction with syntaxin 1a.

EXPERIMENTAL PROCEDURES

DNA Construction—Partial cDNA fragments of mouse phogrin were amplified from the MIN6 cDNA library by PCR using primers 5′-CCATGGACTGAGCGCCAAC-3′ and 5′-TTGTATGGCTCCAGCAACTG-3′, 5′-AGCCACGGTACCTTGTACAT-3′ and 5′-GATGTAGTCGGAACTGCCAT-3′, and 5′-GAATGCACCCAAGAACCGTT-3′ and 5′-CAGGACTGATATCCTGTTGC-3′. The amplified cDNAs were ligated to construct full-length phogrin cDNA. The resultant phogrin cDNA and the enhanced green fluorescent protein (EGFP) cDNA cut from the pEGFP-N2 vector (Clontech, Palo Alto, CA) were simultaneously subcloned into the HindIII and NotI sites of the pcDNA3 vector. Mouse Munc18-1 cDNA similarly was amplified using primers 5′-GAAGACTCGAAGAACGCCAT-3′ and 5′-TGTGGAGCTTGCATGTGAAC-3′ and was cloned into the pcDNA3-HA vector (11). Truncated fragments of syntaxin 1a were constructed by PCR using pGEX-KG-syntaxin 1a-(1–264) (11) as a template and cloned into the same vector. The granuphilin-a mutants W118S and L43A and a recombinant adenovirus bearing each form of granuphilin cDNA were described and characterized previously (11).

Cell Culture and Transfection—MIN6 and AtT20 cell lines were grown in high glucose (25 mM) Dulbecco's modified Eagle's medium supplemented with 10% fetal calf serum except where indicated otherwise. Transfections were performed with LipofectAMINE 2000 reagent (Invitrogen) according to the manufacturer's instructions. MIN6 cells were transfected with the phogrin-EGFP plasmid, and stable clones were selected in the presence of 1 mg/ml G418. Individual clones were evaluated by fluorescence microscopy. Phogrin-EGFP was coimmunolocalized with anti-insulin antibodies (60–90%) (see Fig. 1) as described previously (12).

Antibodies—The rabbit anti-granuphilin antibodies, αGrp-aC that recognizes granuphilin-a (9), αGrp-bC that recognizes granuphilin-b (11), and αGrp-N that recognizes both granuphilin-a and -b (10), were described and characterized previously. The rabbit anti-secretogranin III antibodies (13) were gifts from Drs. M. Hosaka (Gunma University) and T. Watanabe (Asahikawa University School of Medicine). The guinea pig anti-porcine insulin serum was a gift from Dr. T. Matozaki and H. Kobayashi (Gunma University). Anti-syntaxin 1a (HPC-1) mouse, anti-Rab27a mouse, anti-ACTH mouse, and anti-hemagglutinin (anti-HA; clone 3F10) rat monoclonal antibodies were purchased from Sigma, Pharmingen, Biogenesis (Poole, UK), and Roche Diagnostics (Mannheim, Germany), respectively.

Indirect Immunofluorescence Microscopy—Indirect immunofluorescence analysis was performed as described previously (11). Briefly, MIN6/phogrin-EGFP cells (clone 41) cultured on 8-well Lab-Tek chamber slides were fixed with 4% paraformaldehyde and permeabilized with either 0.1% Triton X-100 or ice-cold methanol. The cells then were incubated with primary antibodies followed by indocarbocyanine (Cy3)-conjugated, species-specific anti-IgG secondary antibodies (Jackson ImmunoResearch, West Grove, PA). Intrinsic EGFP and antibody staining signals were observed with confocal microscopes TCS-SP2 (Leica Mikrosystems Vertrieb GmbH, Bensheim, Germany), LSM5 PASCAL (Carl Zeiss, Jena, Germany), and MRC-1024 (Bio-Rad) or with an epifluorescence microscope (BX-50; Olympus Optical Co., Tokyo, Japan) equipped with a SenSys™ charge-coupled device camera (Photometrics, Tucson, AZ).

A peripheral pattern of EGFP signals was quantified under a fluorescent microscope as follows. MIN6/phogrin-EGFP cells were transiently transfected with 0.1 μg of an expression plasmid encoding HA-granuphilin. The cells were incubated under a low glucose condition (2 mM) for 24 h. The cells then were fixed with 4% paraformaldehyde, permeabilized with 0.05% Triton X-100, and incubated with anti-HA rat monoclonal antibodies followed by Cy3-labeled anti-rat IgG. Cells that revealed a linear distribution along a part of the plasma membrane were judged as positive, whereas those that showed only a punctate granular pattern were judged as negative. Cells that showed ambiguous patterns, which constituted ~10% of the cells, were excluded from the counting. Although only Cy3-positive, HA-granuphilin expressing cells were judged in the assay, ~20% of untransfected cells normally show the peripheral pattern of EGFP signals. For each experiment, a total of 100 cells were unambiguously assessed.

Immunoprecipitation and in Vitro Binding Analysis—Immunoprecipitation and immunoblot analyses were performed as described previously (11). *In vitro* translation of HA-tagged proteins was performed using the TnT-coupled reticulocyte lysate system (Promega, Madison, WI). Purified glutathione *S*-transferase (GST)-fused proteins (1 μg) immobilized on 10 μl of glutathione-Sepharose beads were incubated with equal amounts of *in vitro* translated proteins (6–10 μl) in binding buffer (20 mM Tris, pH 7.5, 150 mM NaCl, 2 mM $MgCl_2$, 1 mM EGTA, 0.1% Nonidet P-40) at 4 °C for 3 h. The beads were washed three times, and the bound proteins were subjected to SDS-PAGE and immunoblotting.

Subcellular Fractionation—Cells were suspended in buffer containing 250 mM sucrose, 20 mM HEPES (pH 7.4), 2 mM $MgCl_2$, 2 mM EGTA, and the following protease inhibitors: 1 mM phenylmethylsulfonyl fluoride and 5 μg each of aprotinin, pepstatin A, and leupeptin per ml. The cells were homogenized for 40 strokes by the tight fitting Dounce homogenizer and the cell condition was monitored under a microscope. The total homogenate was centrifuged at 700 × *g* for 10 min to precipitate the nuclear and intact plasma membranes. The resultant supernatant then was centrifuged at 12,000 × *g* for 20 min to separate the heavy organelle fraction including the secretory granules from the cytoplasmic materials. Fractionates were lysed in buffer (20 mM Tris, pH 7.5, 150 mM NaCl, 2 mM $MgCl_2$, 1 mM EDTA, 1% Triton X-100, and the protease inhibitors described above), and equal proportions of each lysate were subjected to SDS-PAGE and immunoblotting analysis.

Transduction of MIN6 Cells with TAT Fusion Proteins—Isolation of TAT-GFP and TAT-H3 was performed as described previously (14). MIN6 cells were transduced for 50 min with 70 μg/ml of TAT fusion proteins, and the cell extracts were prepared as described for the immunoprecipitation experiments.

RESULTS

Granuphilin Promotes Insulin Granule Targeting to the Plasma Membrane—We demonstrated recently that Rab27a and its effector granuphilin are peripherally localized on the membrane of mature dense core granules in pancreatic beta cells and regulate insulin secretion through interaction with the plasma membrane t-SNARE, syntaxin 1a (10, 11). These biochemical studies suggest that granuphilin plays a role in tethering two membranes, secretory granules and the plasma membrane, at the event of exocytosis. To explore this possibility, we morphologically assessed the function of granuphilin by tracing EGFP-labeled granules. A MIN6 cell line first was established that expresses phogrin-EGFP fusion protein, which was shown previously to be properly targeted to insulin granules in pancreatic beta cells (12, 15). Immunostaining analysis confirmed that phogrin-EGFP is almost entirely colocalized with insulin on secretory granules but not on the perinuclear Golgi region (Fig. 1). Using these cells, the motion of insulin granules can be followed

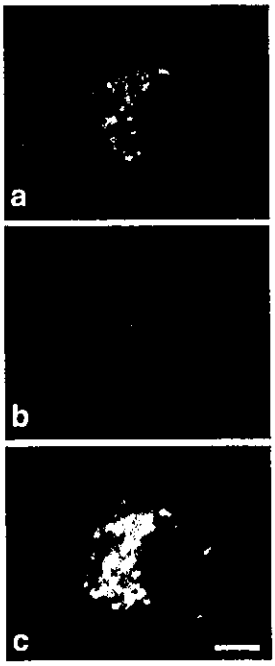

FIG. 1. **Insulin granules are traced by stable expression of phogrin-EGFP in MIN6 cells.** MIN6/phogrin-EGFP cells (clone 41) were fixed and stained with anti-insulin and Cy3-labeled anti-guinea pig IgG antibodies. Intrinsic EGFP fluorescence (*a*), Cy3 fluorescence (*b*), and merged fluorescence (*c*) are shown. *Bar*, 5 μm.

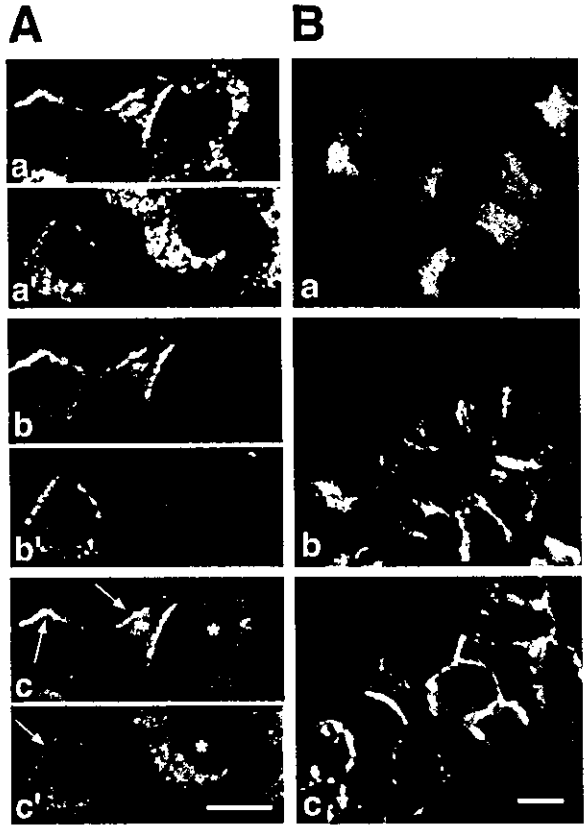

FIG. 2. **Overexpression of granuphilin promotes the targeting of insulin granules to the plasma membrane.** *A*, MIN6/phogrin-EGFP cells were transiently transfected with 0.1 μg of an expression plasmid encoding HA-tagged granuphilin-a. The cells were incubated under a low glucose condition (2 mM) for 24 h. Then they were fixed and immunostained with anti-HA and Cy3-labeled anti-rat IgG antibodies. Intrinsic EGFP fluorescence (*a*, *a'*), Cy3 fluorescence (*b*, *b'*), and merged fluorescence (*c*, *c'*) are shown. Plasma membrane accumulation of EGFP signals was observed at the region marked by *arrows* in cells expressing HA-granuphilin-a. In contrast, neighboring untransfected cells revealed only a punctate granular pattern of phogrin-EGFP-fluorescence (*asterisks*). *B*, MIN6/phogrin-EGFP cells were infected with a recombinant adenovirus bearing β-galactosidase (*a*), granuphilin-a (*b*), or granuphilin-b (*c*) cDNA. The cells were cultured under a high glucose condition (25 mM) and fixed after 12 h. The EGFP fluorescence was observed. *Bars*, 10 μm.

by tracking the EGFP fluorescence. When HA-tagged granuphilin-a was transiently overexpressed, EGFP signals clearly were redistributed at the peripheral region exactly where granuphilin was colocalized (Fig. 2*A*, *arrows*). In contrast, neighboring untransfected cells showed only punctate EGFP signals mainly distributed around the Golgi/endosomal region (Fig. 2*A*, *asterisks*), although some of these normally display a peripheral pattern in this assay condition. These observations suggest that overexpression of granuphilin induces translocation of insulin granules toward the plasma membrane.

Next we used a recombinant adenovirus to express granuphilin more efficiently in MIN6/phogrin-EGFP cells. In our study, almost all cells were infected and expressed exogenous protein (11). Cells infected with the adenovirus that expressed granuphilin-a and -b uniformly exhibited a prominent peripheral redistribution of labeled granules compared with those expressing control β-galactosidase protein (Fig. 2*B*). Granuphilin-b was more effective for the targeting of granules to the plasma membrane. Furthermore, electron microscopic analysis revealed an accumulation of dense core granules near the cell-cell contact region in granuphilin-overexpressing MIN6 cells.[2]

To see these phenomena biochemically, a conventional fractionation procedure was employed. Total MIN6 cell homogenates (T) in sucrose buffer were centrifuged at low speed (700 × *g*) to precipitate the plasma membrane sheets as well as the nucleus (P1). The resultant supernatant then was centrifuged at high speed (12,000 × *g*) to separate the heavy organelles including dense core granules (P2) and other components containing cytosol (S). In control cells expressing β-galactosidase protein, the plasma membrane-associated syntaxin 1a mainly was present in the P1 fraction, whereas peripherally granule-associated Rab27a (10) and the granule content, secretogranin III (SgIII) (13), were distributed in the P2 fraction (Fig. 3, *upper panels*). Overexpression of granuphilin-a by the adenovirus induced significant redistributions of Rab27a and SgIII from P2 to P1, suggesting that insulin granules were moved into the heavier fraction containing the plasma membrane (Fig. 3, *lower panels*). The localization of phogrin, an integral granule-membrane protein, was similar to that of SgIII, and the immunoreactivity of insulin was correlated with these changes (data not shown). Thus, granuphilin overexpression changed the subcellular localization of granule marker proteins. This biochemical finding indicates that the redistributed granules are engaged in distinct molecular interaction rather than simply forced against the membrane. These results, obtained using the adenovirus expression system, strongly suggest that granuphilin facilitates the docking of insulin granules to the plasma membrane.

Granuphilin Promotes ACTH Granule Targeting to the Plasma Membrane—Previous studies have shown that overexpression of granuphilin significantly inhibits high K^+-induced insulin secretion but enhances basal insulin secretion (11, 16). Thus, the peripheral translocation of granules by granuphilin seen in beta cell line MIN6 could be a mere reflection of accumulated granules resulting from the inhibition of secretion, although the phenomenon was observed in both nonstimulatory (Fig. 2*A*) and stimulatory glucose concentrations (Fig. 2*B*). To exclude this possibility, we examined the effect of granuphi-

[2] H. Yokota-Hashimoto, S. Torii, and T. Izumi, unpublished observations.

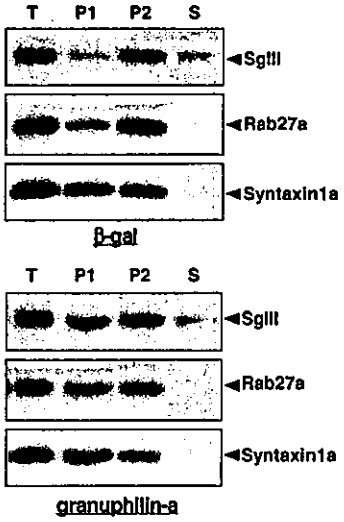

FIG. 3. **Granuphilin induces the redistribution of endogenous granule marker proteins.** MIN6 cells were infected with an adenovirus bearing either β-galactosidase (*upper panels*) or granuphilin-a (*lower panels*) cDNA. The cells were extracted and fractioned by the method described under "Experimental Procedures." Equal proportions of the fractions were analyzed by immunoblotting with antibodies for SgIII, Rab27a, or syntaxin 1a. The subcellular fractions are designated as follows: *T*, total homogenate; *P1*, plasma membrane and nucleus; *P2*, granules and heavy organelle; *S*, cytosol.

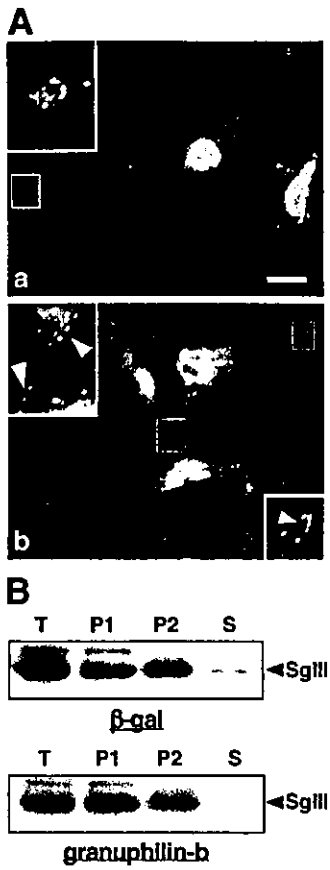

FIG. 4. **Overexpression of granuphilin promotes the targeting of ACTH granules to the plasma membrane.** *A*, AtT20 cells were infected with a recombinant adenovirus bearing β-galactosidase (*a*) or granuphilin-b (*b*) cDNA. The cells were fixed after 48 h and immunostained with anti-ACTH and fluorescein isothiocyanate-labeled anti-mouse IgG antibodies. The peripheral line-up of secretory granules was observed at the region marked by *arrowheads*. *Bar*, 10 μm. *Insets* show the higher magnification (×3.2) pictures within the *boxed areas*. *B*, AtT20 cells infected with the adenovirus were extracted and fractioned as in Fig. 3. Equal proportions of the fractions were analyzed by immunoblotting with antibodies for SgIII. *T*, total homogenate; *P1*, plasma membrane and nucleus; *P2*, granules and heavy organelle; *S*, cytosol.

lin overexpression in pituitary corticotroph cell line AtT20. This cell line also physiologically expresses Rab27a/b and granuphilin (17) and does not stimulate hormone secretion in response to a high glucose level in custom medium, which is in contrast to MIN6 cells. In addition, a relatively lower density of granules in the peripheral cytoplasm of AtT20 cells enabled us to distinguish each ACTH-positive spot. Cells infected with adenovirus expressing granuphilin-b again induced a redistribution of granules along the plasma membrane (Fig. 4*A*). Furthermore, as with MIN6 cells, biochemical fractionation analysis showed that granule marker proteins such as SgIII are significantly redistributed in these cells (Fig. 4*B*). Taken together, these results indicated that the peripheral redistribution of granules by granuphilin overexpression does not simply reflect its inhibitory effect on secretion.

Granuphilin Co-works with Syntaxin 1a on the Peripheral Targeting of Insulin Granules—We demonstrated previously that granuphilin is partially colocalized with and directly binds to syntaxin 1a in pancreatic beta cells (11). Because syntaxin 1a is one of the SNARE proteins on the plasma membrane that mediates the membrane fusion reaction, granuphilin may tether insulin granules to the exocytotic site by an association with syntaxin 1a. To explore this possibility, first we examined the intracellular localization of syntaxin 1a and EGFP-labeled granules that are redistributed to the plasma membrane in the granuphilin-overexpressing cells. The peripheral localization of labeled granules overlapped well with the local distribution of syntaxin 1a in cells overexpressing granuphilin-b (Fig. 5*A*).

Next we examined the targeting activities of granuphilin mutants that are defective in binding to either Rab27a or syntaxin 1a. We demonstrated previously that the W118S and L43A mutations specifically disrupt interactions of granuphilin with Rab27a and syntaxin 1a, respectively (11). Overexpression of neither W118S nor L43A altered the distribution of granules labeled by phogrin-EGFP in contrast to wild-type granuphilin-a (Fig. 5*B*). Some of the W118S-expressing cells showed a more compact, Golgi-like EGFP fluorescence pattern compared with control cells. Immunostaining of the W118S mutant revealed a diffuse cytosolic distribution, which may reflect the inert binding activity of this mutant to Rab27a (data not shown). Although it is difficult to evaluate the targeting activities quantitatively, cells with peripheral distribution of EGFP signals were counted in conventional transfection assays (under "Experimental Procedures"). Wild-type granuphilin-a and granuphilin-b showed 59 ± 5% and 76 ± 4% (mean ± S.E., $n = 4$) targeting activity, respectively. In contrast, W118S and L43A mutants displayed much lower activity, 21 ± 3% and 27 ± 6%, respectively, which is comparable with levels found in control cells (20 ± 2%). These observations suggest that interactions with both Rab27a and syntaxin 1a are required for the targeting function of granuphilin.

Transduction of MIN6 Cells with TAT-fused H3 Fragment of Syntaxin 1a Inhibits the Plasma Membrane Docking of Insulin Granules and the Formation of Granuphilin-Syntaxin 1a Complex—Ohara-Imaizumi *et al.* (14) recently examined the effect of a TAT-fused H3 fragment of syntaxin 1a on the exocytosis of insulin granules in MIN6 cells using an evanescent wave microscopic technique. Human immunodeficiency virus-1 TAT protein can cross a biological membrane efficiently and promote delivery of fused peptides into cells. Ohara-Imaizumi *et al.* (14) showed that the introduction of TAT-H3 inhibits the plasma membrane docking of newly arrived insulin granules as well as the membrane fusion of predocked granules. These findings suggest that syntaxin 1a is required for replenishment of insulin granules into the docked pool. Combined with the

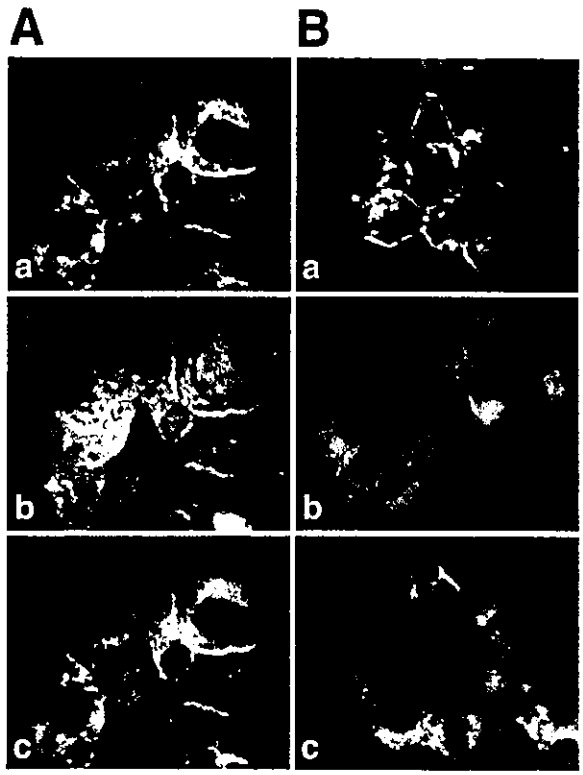

FIG. 5. **Granuphilin targets secretory granules to the plasma membrane by the interaction with syntaxin 1a.** *A*, MIN6/phogrin-EGFP cells were infected with recombinant adenovirus bearing granuphilin-b and fixed after 12 h. The cells were permeabilized with methanol and immunostained with anti-syntaxin 1a and Cy3-labeled anti-mouse IgG antibodies. Intrinsic EGFP fluorescence (*a*), Cy3 fluorescence (*b*), and merged fluorescence (*c*) are shown. *B*, MIN6/phogrin-EGFP cells were infected with a recombinant adenovirus encoding wild-type granuphilin-a (*a*) or its point mutants, W118S (*b*) and L43A (*c*), and were examined for the plasma membrane targeting of EGFP signals.

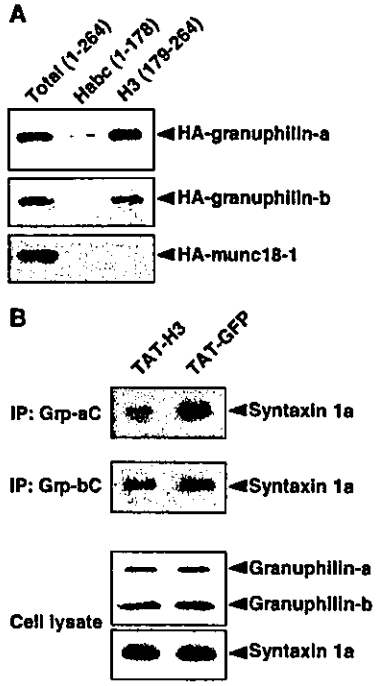

FIG. 6. **Transduction of H3 fragment of syntaxin 1a reduces a native granuphilin-syntaxin complex in MIN6 cells.** *A*, the GST-fused syntaxin 1a total fragment (1–264 amino acids), N-terminal fragment (1–178 amino acids), or C-terminal fragment (179–264 amino acids) were incubated with *in vitro* translated, HA-tagged granuphilin-a, granuphilin-b, or Munc18-1. Proteins that bound to the GST fusion proteins were analyzed by immunoblotting with anti-HA antibodies. *B*, TAT-syntaxin H3 or control protein TAT-GFP was transduced into MIN6 cells as described under "Experimental Procedures." Cell extracts were incubated with either anti-granuphilin-a (αGrp-aC) or anti-granuphilin-b antibodies (αGrp-bC). Each immunoprecipitate (*IP*) was analyzed by immunoblotting with antibodies against syntaxin 1a. The expression levels of endogenous proteins in each cell lysate were determined by immunoblotting with anti-granuphilin antibodies (αGrp-N) and anti-syntaxin 1a antibodies.

present findings, we thought that the reduced docking of granules by TAT-H3 might result from direct competitive interaction with granuphilin between the H3 fragment and the endogenous syntaxin 1a. First we tested which domain in syntaxin 1a is responsible for the interaction with granuphilin. Recombinant GST-fused syntaxin fragments were produced and incubated with HA-tagged granuphilins translated *in vitro*. In this direct binding assay, both granuphilin-a and -b bound to a C-terminal region of syntaxin 1a including the H3 domain as well as its total cytoplasmic region, but not to an N-terminal region including the Habc domain (Fig. 6*A*). In contrast, HA-Munc18-1 was coprecipitated with the full cytoplasmic region of syntaxin 1a but not with the N-terminal or C-terminal fragment as reported previously (18).

Next we introduced TAT-H3 peptides into MIN6 cells and confirmed that they significantly reduce the docking of newly recruited granules as shown previously (14) (data not shown). On this condition, we examined whether TAT-H3 treatment causes dissociation of the endogenous granuphilin/syntaxin 1a complex. After incubating cells with TAT proteins for 50 min, cell extracts were prepared for coimmunoprecipitation experiments. When TAT-H3 was introduced, the amount of syntaxin 1a coprecipitated with anti-granuphilin-a or anti-granuphilin-b antibodies was significantly decreased as compared with the case of control TAT-GFP (Fig. 6*B*). The expression levels of granuphilins and syntaxin 1a were not influenced in this condition. We could detect only a small amount of complex between the TAT-H3 peptide and endogenous granuphilin using transduced MIN6 cell lysate. It is, however, difficult to use metal-binding beads for sedimentation of the His_6-tagged TAT peptide because efficient interaction of these proteins requires a chelator.[3] Taken together, these data suggest that both granuphilin and syntaxin 1a are involved in tethering of insulin granules to the exocytotic site in the plasma membrane, possibly through a direct interaction.

DISCUSSION

The slow and biphasic kinetics of insulin secretion from pancreatic beta cells often is explained by the small population of docked granules and the subsequent steps in which a number of granules are moved and targeted to the plasma membrane (4, 19). The targeting process of secretory granules, however, has not been characterized in part because of the absence of obvious vesicle docking sites such as the active zone in neural cells. In the present study, we suggest that granuphilin is a regulator for the plasma membrane targeting of insulin granules in cooperation with Rab27a and syntaxin 1a. Granuphilin efficiently promotes a peripheral redistribution of insulin granules, which likely represents a physiological targeting event because the same peripheral distribution was observed in some cells without overexpression of granuphilin. Our previous demonstration that granuphilin directly and specifically binds to Rab27a and syntaxin 1a suggests that granuphilin tethers insulin granules and the plasma membrane through these interactions (10, 11, 20). Consistently, two kinds of granuphilin mutants that have a defect in binding to

[3] S. Torii and T. Izumi, unpublished observations.